Biomass and Bioenergy 119 (2018) 392–410

Contents lists available at ScienceDirect

Biomass and Bioenergy

journal homepage: www.elsevier.com/locate/biombioe

Research paper

Influence of biomass torrefaction parameters on fast pyrolysis products under flame-equivalent conditions

S. Pielsticker[a,*], G. Möller[a], B. Gövert[a], T. Kreitzberg[a], O. Hatzfeld[a], Ö. Yönder[b], V. Angenent[c], C. Hättig[b], R. Schmid[c], R. Kneer[a]

[a] Institute of Heat and Mass Transfer (WSA), RWTH Aachen University, Augustinerbach 6, 52056, Aachen, Germany
[b] Chair of Theoretical Chemistry, Group of Quantum Chemistry, Ruhr-University Bochum, Universitätsstraße 150, 44780, Bochum, Germany
[c] Chair of Inorganic Chemistry II, Group of Computational Materials Chemistry, Ruhr-University Bochum, Universitätsstraße 150, 44780, Bochum, Germany

ARTICLE INFO

Keywords:
Torrefaction
Fast pyrolysis
Beech wood
Miscanthus
Fluidized bed
FTIR

ABSTRACT

Pretreating raw biomass via torrefaction changes fuel specific properties like grindability, volatile content, energy density and biochemical stability and thus enables an enhanced fuel replacement for pulverized fossil fuel fired furnaces.

In this study, the influence of torrefaction temperature on devolatilization behavior is investigated in a small-scale fluidized bed reactor approximating flame-equivalent conditions. Therefore the pyrolysis products of two different biofuels with varying degree of torrefaction are determined via ex-situ FTIR gas analysis in an N_2 atmosphere in the temperature range from 873 to 1473 K. Furthermore, the mass fraction of residual char particles is determined by adding O_2 to the fluidizing gas and analyzing the burnout products. Char fraction and volatile composition are used to estimate the energy release distribution between homogeneous volatile combustion and heterogeneous char burnout.

The experiments revealed enlarging char yields at the expense of volatile yields with increasing degree of torrfaction at all investigated pyrolysis temperatures. Furthermore, torrefaction favors higher fractions of CO_2 and lower fractions of CO and C_2H_x in the light gas. Further on, no significant impact of torrefaction conditions on the tar composition could be identified. The calculation of higher heating value (HHV) based on char yield and gas composition reveals an overall increase of HHV, while the relative contribution from the volatile fraction decreases with increasing degree of torrefaction. Following this, an increase of torrefaction degree will shift combustion from a high intense volatile combustion in the near burner region towards a less intense but prolonged char conversion in the far burner region.

1. Introduction

The usage of solid biogenic fuels as alternative fuels in coal-fired pulverized fuel boilers can reduce net carbon emissions of power plants [1] and allows for a negative carbon balance when carbon capture and storage (CCS) technologies are applied. The main technical drawbacks in replacing conventional fossil fuels with biomass are the divergent fuel properties of biomass, especially higher volatile content, lower energy density, fibrous structure, lower biostability, and inhomogeneity. A thermal pretreatment via torrefaction helps to improve those properties to generate a more coal-like biogenic fuel [2].

For design and optimization of torrefied biomass-fired furnaces (e.g. Li et al. [3]), detailed knowledge of the pyrolysis/devolatilization product distribution is required to predict ignition behavior, pollutant formation and energy release from volatile combustion in the near-burner region. The pyrolysis product distribution depends on pretreatment parameters (torrefaction temperature, residence time) and on pyrolysis conditions such as temperature, heating rate and residence time.

Table 1 lists experimental studies investigating the influence of different torrefaction conditions on the product distribution during pyrolysis. There is a general consensus in these studies that an increased degree of torrefaction favors the formation of solid char and reduces the amount of released liquid products, either called tar or bio-oil. Regarding the amount of released non-condensable gases, different dependencies on the degree of torrefaction are evident. An overall slight tendency can be identified that lower pyrolysis temperatures favor an increased gas yield with increasing degree of torrefaction, while higher

* Corresponding author.
E-mail address: pielsticker@wsa.rwth-aachen.de (S. Pielsticker).

https://doi.org/10.1016/j.biombioe.2018.08.014
Received 12 March 2018; Received in revised form 30 July 2018; Accepted 29 August 2018
0961-9534/ © 2018 Elsevier Ltd. All rights reserved.

Table 1
Literature overview of experimental studies investigating pyrolysis products of biomass samples with varying degree of torrefaction in comparison to the raw material.

Reference	Fuel	Torrefaction conditions		Pyrolysis conditions		Behavior of pyrolysis products with increasing degree of torrefaction[a]								
		Temp. [K]	Time [min]	Temp. [K]	Heating rate	Gas	Tar	Char	H_2O	CO	CO_2	CH_4	H_2	$C_{2+}H_x$
Barontini et al. [4,5]	Palm kernel shell	473–573	30	up to 900	20 K min^{-1}				y↘	y↘	y↘			
				1173	high					c↘	c↷	c↘	c↷	c↘
Boateng et al. [6]	Hardwood, switchgrass	undefined		unknown	high	y↗	y↘	y↘						
Cen et al. [7]	Corn stalk	523	30	773	high	y↘	y↘	y↘		c↘	c↘	c→	c↘	c→
Chen et al. [8–10]	Rice husk, cotton stalk, pine	473–563	30	773	high	y↷	y↘	y↘						
				773	high	y↷	y↘	y↘		c↘	c↘	c↘	c↘	c↷
				823	high	y↘	y↘	y↘		c↘	c↘	c↷	c↘	c↷
Li et al. [11]	Palm kernel shell	473–573	30	1173	$10^4 - 10^5$ K s^{-1}	y↘	y↘		c↷	c↷	c↷	c↷	c↘	
Louwes et al. [12]	ash wood, spruce	523–553	45	773	high					c↘	c↘		c↘	
Raut et al. [13]	Poplar	523–573	60	1073	high	y↘	y↘	y↘						
Ren et al. [14]	Douglas fir sawdust	513–583	8–22	753	unknown	y↘	y↘	y↘		c↘	c↘	c↘	c↷	
Ru et al. [15]	Poplar	473–573	30	up to 1173	10 K min^{-1}			y↘						
Tsalidis et al. [16,17]	Spruce, ash wood	563–573	20–30	773–1273	600 K s^{-1}	y(T)	y(T)	y↘		y(T)	y(T)	y(T)		
				873–1273	600 K s^{-1}	y↘	y↘	y↘		y(T)	y(T)	y(T)	y(T)	
Wafiq et al. [18]	Miscanthus	523	30	1073	800 K s^{-1}	y↘	y→	y↘		y↘	y↘	y↘	y→	y→
Wannapeera et al. [19]	Leucaena Leucocephala	473–593	0–1140	up to 1073	10 K min^{-1}	y↘	y↘	y↘	y↘	y→	y↘	y→		
Xin et al. [20]	Licorice residue	483–553	60	723–1073	2×10^4 K s^{-1}					c↘				
Zhang et al. [21–23]	Rice husk	483–583	30–60	823	high	y↘	y↘	y↘		c↘	c↘	c↘	c↘	c→
Zheng et al. [24–27]	Pine, corncobs, hemicellulose, cellulose, lignin	483–593	10–60	793	high	y↷	y↘	y↘						
				743	high	y→	y↘	y↘						
				873	2×10^4 K s^{-1}	y↘	y↘	y↘						

[a] y: mass yield c: gas concentration ↘: strong increase ↘: slight increase →: constant ↘: slight decrease ↘: strong decrease ↷: maximum ↷: minimum (T): function of pyrolysis temperature.

pyrolysis temperatures favor a decreasing gas yield. Regarding the release behavior of individual gas species, the discrepancies between the different studies are much more pronounced.

To characterize both – the impact of torrefaction and pyrolysis conditions – temperature dependent studies are required, which only have been undertaken by Tsalidis et al. [16,17] and Xin et al. [20]. The lack of experimental data for biomass with a varying degree of torrefaction undergoing pyrolysis processes at high temperatures and high particle heating rates was already identified by Barontini et al. [5] but has not been remedied yet.

The objective of this study is to close the identified gap in the currently available experimental data. To achieve this, the impact of torrefaction temperature on fast pyrolysis yields and gas composition under conditions similar to those in the ignition zone of pulverized fuel boilers is investigated. The yields of 22 single gas species are calculated from an FTIR gas analysis in the exhaust gas stream of a batchwise operating small-scale fluidized bed reactor, which has already been used for several pyrolysis studies [28–30]. Experiments have been undertaken in the temperature range from 873 to 1473 K at high particle heating rates of approximately 5×10^4 K s^{-1} for two different fuels and two different degrees of torrefaction per fuel, to quantify both: the influence of torrefaction and pyrolysis conditions on the gas yields.

The data presented in this study has two main usage scenarios: It can be used to improve the prediction of the higher heating value of pyrolysis products released from torrefied biomass depending on the torrefaction- and pyrolysis conditions. And the data can also serve as a basis for adapting available network pyrolysis models for coal to the pyrolysis process of torrefied biomass.

2. Material and methods

The experimental investigation performed in this study can be divided into three main steps: fuel pretreatment, fuel analysis, and determination of fast pyrolysis products. In the first step, raw biomass is transformed into torrefied biomass under different conditions by using a small-scale continuously working screw reactor. In the second step, the torrefied product is analyzed, ground and sieved into different particle size fractions. And in the third step, one of these fractions is fed batchwise into a small-scale fluidized bed reactor to investigate fast pyrolysis yields under flame-equivalent conditions.

2.1. Raw fuel characterization

In the present study, two different biogenic fuels are investigated. Beech wood (*Fagus sylvatica*) is chosen as a representative for woody biomass and miscanthus (*Miscanthus × giganteus*) as a representative for stalk biomass, respectively. Both biomasses have been cultivated in northern Germany and have been acquired from industrial manufacturers (Beech wood: *Goldspan GmbH & Co. KG*, Miscanthus: *Miscanthus OppStock GbR*). Both materials constitute a mix of plants harvested at different plant ages. Mechanical pretreatment undertaken by the manufacturer resulted in beech wood chips with typical dimensions of 10 × 10 × 2 mm and shredded miscanthus with strongly elongated particles up to 5 cm in length. The material has been stored in sealed plastic bags until use in the laboratory.

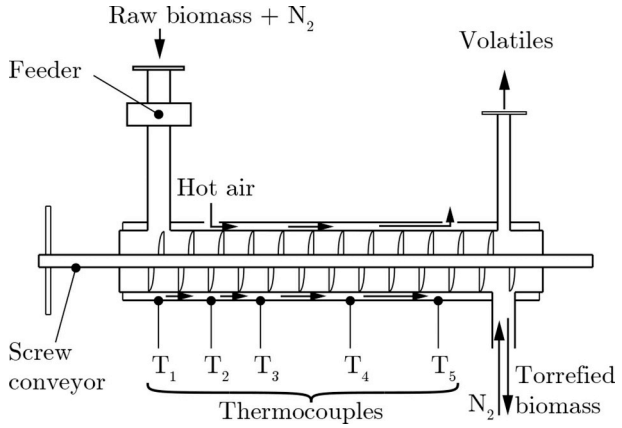


Fig. 1. Scheme of the continuously working screw reactor for torrefaction.

2.2. Fuel pretreatment by torrefaction

Before the raw materials are torrefied, they are dried in a conventional dryer at 379 K (*Heraeus UT 5042*) for 2 h to ensure comparable moisture contents of the used samples.

Torrefaction is performed in a continuously working screw reactor shown in Fig. 1 and described in detail by Ohliger et al. [31]. The reactor consists of two co-axial stainless steel pipes and a screw conveyor with a length of 1000 mm and a diameter of 160 mm. Heating is realized indirectly by hot air flowing through the annular gap between the two pipes in co-current flow with the biomass. Temperature is controlled via the thermocouples 2–5, which are mounted to the wall of the inner pipe. An exemplary temperature profile is given in Ohliger et al. [31]. Biomass is delivered to the screw conveyor through a rotary feeder. The screw conveyor allows precise control of the biomass residence time in the reactor. Both, the rotary feeder and the screw conveyor are driven by individual electrical motors, which allows controlling mass flow and residence time individually. Nitrogen (purity 99.998 vol.-%) is applied to the storages (not shown) for both, raw and torrefied biomass as well as to the reactor itself, ensuring an inert atmosphere to avoid combustion. Additionally, this setting forces the volatiles to escape through the intended outlet. In the present study, the torrefied material is produced under two different operating conditions. In the first run the torrefaction set temperature is 553 K and in the second run, it is 573 K. The two temperatures have been chosen as in this temperature range a strong decomposition of hemicellulose is expected. All other parameters are kept constant for both runs. Residence time is set to 30 min via controlling the rotation speed of the screw conveyor and fuel feed rate is set to 2 kg h^{-1} via controlling the rotation speed of the rotary feeder.

2.3. Fuel characterization methods

Following the torrefaction process, samples are ground with a *Retsch SM 100* cutting mill and sieved afterward with a *Retsch AS 200* sieving machine. For further analyzes and investigations of fast pyrolysis yields the mesh size fraction 90–125 µm is used. Milled and sieved samples of raw and torrefied biomass are analyzed with standardized testing procedures. Proximate analysis was undertaken with muffle furnace *Nabertherm* L*5/13/B410* and drying cabinet *Heraeus 5000 Series* to obtain moisture (DIN 51718 [32]), volatile (DIN 51720 [33]) and ash (DIN 51719 [34]) content. Analogously a *Leco TruSpec Micro CHNS* is used for determination of C, H, N and S content (DIN 51732 [35], DIN 51724 [36]). Particle size analysis is undertaken with an *Olympus SZ-40* zoom stereo microscope combined with a *Nikon D5100* digital camera and a self-developed MATLAB-based image analysis software. Due to the elongated shape of the particles, a cylindrical particle model is used to determine equivalent particle diameter and length. Further details

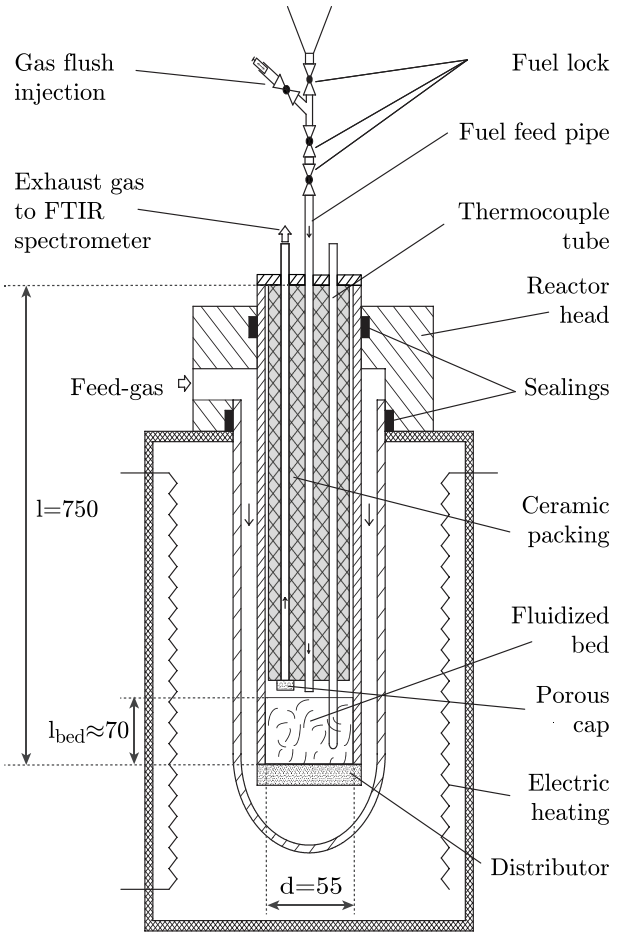


Fig. 2. Scheme of the fluidized bed reactor for pyrolysis experiments (dimensions in mm).

are presented in Appendix A.

2.4. Fluidized bed reactor for fast pyrolysis

Pyrolysis experiments are conducted batchwise in a fluidized bed reactor (FBR), which is described in detail by Haustein et al. [37] and Pielsticker et al. [29]. The reactor is located in an electrically controlled furnace to set the surrounding temperature individually. As shown in Fig. 2, the reactor consists of two coaxial ceramic pipes, which are mounted to the stainless steel reactor head. The feed gas enters the reactor through the reactor head and is guided downwards through the annular gap between the pipes before it flows through a distributor to fluidize the bed in the inner pipe. For all experiments, the flow rate is set to 100 L_{STP} h^{-1} (standard conditions) nitrogen 4.8 (purity 99.998 vol.-% N_2). The porous distributor is made from sintered silica glass with a pore size range of 40–100 µm providing a homogeneous inflow. The bed consists of Al_2O_3 particles with a diameter d_{50} = 141 µm (mesh size 112–180 µm).

For each run a fuel sample (m_{fuel} = 15 mg) is injected batchwise into the reactor through fuel lock and fuel feed pipe. Driven by gravity and an additional nitrogen flush of 10 mL the fuel is transported to the fluidized bed. The fuel particles heat up with an initial (peak) heating rate of approximately 5×10^4 K s^{-1} and release devolatilization products. Depending on particle size and fluidized bed temperature, the actual range of calculated initial heating rates varies from 0.95×10^4 to 14×10^4 K s^{-1}. The heating rate has been analytically approximated using an energy balance for a single particle inside the fluidized bed, accounting for radiative and convective heat transfer. The basic model is presented in Gövert et al. [38]. For the current calculation, it is

further assumed that the particles enter the fluidized bed already preheated to 573 K and that any cooling effect due to the pyrolysis reaction is negligible for the initial heating rate. The gaseous products are captured above the bed and transported to a Fourier-transform infrared spectrometer (FTIR) via a heated (453 K) sampling line to avoid condensation of tars and water vapor. The tip of the sampling line inside the reactor is equipped with a sintered quartz glass cap to reduce entrainment of particles. It consists of the same material as the distributor plate and causes – along with the FTIR, the gas cell and a further particle filter – a pressure drop. Hence, the reactor is run at a slight overpressure of 10–50 mbar. The upper part of the inner pipe above the fluidized bed is blocked by a ceramic packing. This prevents mixing of pyrolysis products and base gases within the dead volume above the bed and leads to shorter residence times of the gases in the reaction zone and reduces secondary reactions. As the blocking was installed after the beech wood experiments, only miscanthus experiments were conducted with shorter gas residence times. A method for estimating the different gas residence time distributions of both setups is presented in section 2.6.

The FTIR spectrometer in use is a *Ansyco Gasmet DX-2000*, which is measuring in the wave number range of 600–4200 cm^{-1}. Spectra are recorded with a sampling rate of 0.5 Hz. The accuracy given by the manufacturer is 2% of the measurement value. The system is used for analyzing pyrolysis products and the chemical composition of the remaining char particles. The latter is measured by adding O_2 to the fluidizing gas, burning the particles and measuring the burnout products.

Pyrolysis experiments were undertaken for each fuel in the temperature range of 873–1473 K with a step size of 100 K. For each operation point, the single experiment is repeated ten times and a mean value is calculated. The resulting standard deviation of the repetitions is marked as error bars in the figures presented later on.

2.5. Evaluation procedure

The evaluation procedure is separated into three steps: multivariate regression, noise filtering and mass-specific yield calculation.

Time-dependent concentration profiles for each species are extracted from the measured raw spectra via multivariate regression using proprietary software Calcmet™ (version 11.118). The selection of potential relevant gas species was done according to the procedure developed in Pielsticker et al. [29], capturing peak concentration of the pyrolysis process in an enclosed gas cell and analyzing gas concentrations over several minutes to reduce the influence of noise. This optimization procedure of selected gases was once performed including spectra from pyrolysis experiments of raw beech wood at 873 K and 1373 K. The chosen selection of 22 potential pyrolysis gases was then kept constant for all other experiments. Corresponding wave number regions for the evaluation are given in Pielsticker et al. [29].

The predefinition of selected gas species in the beginning is required to limit the evaluation effort although it might not be the optimum gas selection for each experiment. In consequence, the signal of a gas can be reliable in one experiment but may just be noise in another. To prevent the misinterpretation of noise as species yield, a filter is applied to the concentration profiles in the second step of the evaluation procedure.

The most common criterion to distinguish between a signal originating either from noise or IR gas absorption is the signal-to-noise ratio (SNR). In the current use case, SNR is defined as the maximum concentration divided by the standard deviation of the concentration signal in a time span, where no absorption signal is expected (e.g. before a fuel sample is injected). Due to the fact that regression analysis with Calcmet™ restricts negative concentration values (except for H_2O and CO_2), this method turned out to be quite unstable. Therefore an optimized method for the distinction between noise and IR absorption was implemented. The necessary assumption for this is that all pyrolysis reactions take place much faster than the gas exchange rate. Following this, all species will qualitatively show a similar concentration profile. A normalization to the peak value should result in almost identical profiles if SNR is sufficient. Fig. 3 shows exemplary normalized concentration profiles for methane (CH_4) and ethane (C_2H_6) for pyrolysis experiments of raw beech wood at 873 K (left) and 1273 K (right). Due to high SNR in all experiments, CH_4 was chosen as reference species. The dark gray area shows intersection between normalized CH_4 and C_2H_6 signals. At 873 K, the intersection area is 85% of the light gray marked area under the CH_4 peak. In contrast, this reduces to 22% at 1273 K. Based on visual inspection of a large number of signals, species with an intersection area of less than 30% can reliably be identified as pure noise and were hence ignored for further analysis.

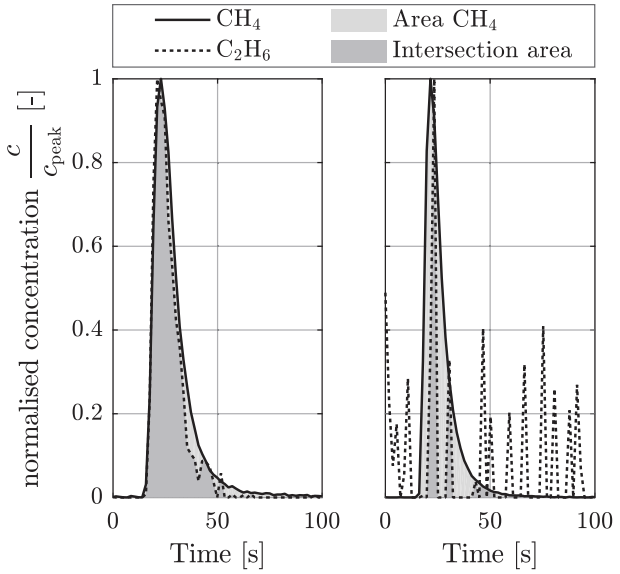


Fig. 3. Normalized concentrations of CH_4 and C_2H_6 of raw beech wood with intersection area as a criteria to differentiate between IR absorption and noise, left: C_2H_6 absorption at 873 K (intersection area 85%), right: noise at 1273 K (intersection area 22%).

In the final evaluation step, mass-specific yields of gaseous pyrolysis products and solid char residue are calculated. Fig. 4 shows a typical CO_2 concentration curve for one single pyrolysis experiment and the subsequent char burning process.

The yield y_i of any species i in $kg_i\,kg_{fuel}^{-1}$ can be calculated from the

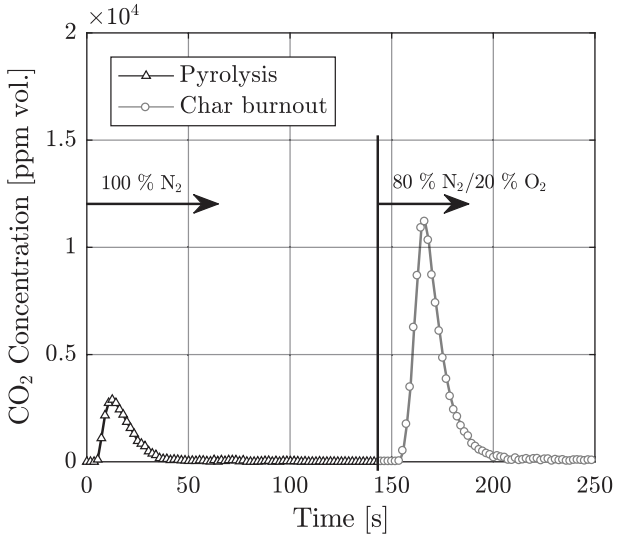


Fig. 4. Concentration profile of CO_2 in pyrolysis and char burnout step for torrefied beech wood (573 K) at 1473 K.

dedicated volumetric concentration $c_i(t)$, the feed gas volume flow $\dot{V}_{N_2}$ and density ρ_{N_2} for standard conditions ($T = 273$ K, $p = 101.325$ kPa), the molar mass of nitrogen M_{N_2} and species M_i and the delivered fuel mass m_{fuel} according to equation (1):

$$y_i = \frac{\rho_{N_2}}{m_{fuel}} \frac{M_i}{M_{N_2}} \cdot \int_{t_{start}}^{t_{end}} \frac{\dot{V}_{N_2}(t)}{1 - \sum_{j=1}^{n} c_j(t)} \cdot c_i(t) \mathrm{d}t \tag{1}$$

This equation is based on the assumption that the fluidizing gas consists of pure nitrogen, all produced gas is passing the FTIR and all gases can be treated according to the ideal gas law. Furthermore, the effect of an enlarged volume flow due to the evolved pyrolysis gases is considered by the factor $(1 - \sum_{j=1}^{n} c_j)^{-1}$. To estimate the tar yield, gas yields of species with a condensation temperature over 293 K, except water vapor, are summed up.

The yield of remaining char is determined by adding oxygen to the fluidizing gas, burning off the char particles, measuring the concentration profiles of the reaction products (CO_2, CO, H_2O, SO_2 and NO_x) like it can be seen for CO_2 in Fig. 4 and calculating specific product gas yields in analogy to equation (1). Under the assumption that the oxygen content in the char can be neglected, the mass fraction of the solid residue can be estimated via an elemental mass balance for carbon, hydrogen, sulfur and nitrogen.

Due to some particle entrainment, particles sticking in the feed pipe, condensation of heavy tars and a lack of H_2 detection, the mass balance cannot be closed completely. For a better comparison, each yield is normalized to the total mass recovery of the respective single experiment.

2.6. Estimation of gas residence time distribution

To visualize the impact of the installed ceramic packing, a gas residence time distribution analysis is undertaken. Equation (2) gives the relative mass yield as a function of yield $y(t)$ at time t divided by the final yield y_∞ under the simplifications that fluidizing volume flow is constant over time and concentration of pyrolysis gas is small compared to the concentration of N_2 base flow.

$$\frac{y(t)}{y_\infty} \approx \frac{\sum_{i=1}^{n} M_i \cdot \int_{t_{start}}^{t} c_i(t) \mathrm{d}t}{\sum_{i=1}^{n} M_i \cdot \int_{t_{start}}^{t_\infty} c_i(t) \mathrm{d}t} \tag{2}$$

Fig. 5 gives the relative mass fraction passing the FTIR gas cell between time t_{j-1} and t_j. A non-uniform time division is chosen to sum mass fractions of at least 2.5%. Exemplarily the results from experiments of raw fuels at a reactor temperature of 1173 K are shown, but no big influence of reactor temperature on residence time distribution can be obtained at other temperatures. A much bigger difference can be observed between the distribution from the setup without ceramic packing used for beech wood experiments and those with ceramic packing used for miscanthus experiments. The improved setup with packing increases the relative mass fraction with residence times shorter than 10 s and reduces mass fractions with residence times above 20 s significantly. The overall shorter residence time in the improved setup with packing reduces secondary reactions, ending in higher tar and lower gas yields compared to the setup without ceramic packing. A more detailed discussion of this phenomenon can be found in section 3.3.

3. Results

To evaluate the potential of torrefied biomass instead of raw biomass as a fuel in pulverized fuel boilers, the impact of torrefaction on the following properties is analyzed:

- **Basic fuel properties** (sec. 3.1) like elemental composition and particle size distribution e.g. for prediction of grindability.

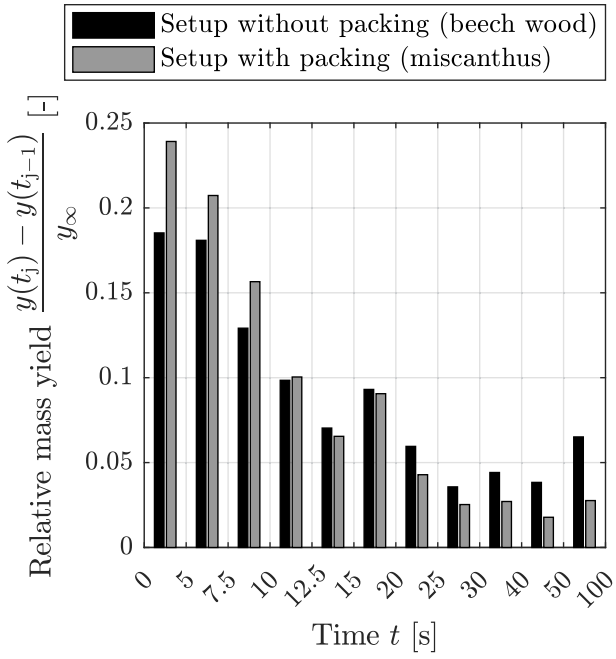


Fig. 5. Gas residence time distribution calculated based on relative mass yield for setup without ceramic packing (beech wood) and setup with ceramic packing (miscanthus) at 1173 K.

- **Residual char yield** (sec. 3.2) and **volatile yield** (sec. 3.3) to determine the individual influence of the heterogeneous and homogeneous combustion processes.
- **Volatile composition** divided into tar (sec. 3.4) and gas (sec. 3.5) fraction to identify possible precursors of pollutant emissions and better understand underlying chemical processes (cf. sec. 3.6)
- **Heating value** (sec. 3.7) of char and volatile gases to quantify the ratio of heat release during volatile combustion and char burnout.

An analysis of the listed properties is possible thanks to the detailed data on 22 species gathered from FTIR analysis. The temperature dependent yields of 20 gas species[1] are also presented in full detail in the section Appendix B. The individual pyrolysis gas yields are intended as a helpful reference for the further development of network pyrolysis models for biogenic fuels.

3.1. Basic fuel properties

Table 2 summarizes results from proximate, ultimate and microscopic particle size analysis. Raw and torrefied material with torrefaction temperatures of 553 K and 573 K for beech wood and miscanthus combined result in a total of six investigated fuels.

The progress of decomposition is defined by the torrefaction degree $\phi_{\Delta m}$, which is given by

$$\phi_{\Delta m} = \frac{\Delta m}{m_0}, \tag{3}$$

where Δm is the mass loss during the torrefaction process and m_0 the initial injected sample mass, both in dry ash free base [31]. For both biomass types, the degree of torrefaction increases with torrefaction temperature. Furthermore, other effects concerning elemental composition or grindability can be linked to the degree of torrefaction. Torrefaction also leads to an increase in the carbon content and a decrease

[1] The yields of SO_2 and methanol are excluded from the plots. Only small traces of SO_2 and methanol have been detected below 1173 K and at 873 K respectively.

Table 2
Physical and chemical properties of raw and torrefied (T_{torr} = 553 K and T_{torr} = 573 K) beech wood and miscanthus according to ultimate, proximate and microscopic particle size analysis for mesh size fraction 90–125 µm.

	Unit	Basis	Beech wood			Miscanthus		
			Raw[f]	T_{torr} = 553 K	T_{torr} = 573 K	Raw[f]	T_{torr} = 553 K	T_{torr} = 573K
Degree of torrefaction $\phi_{\Delta m}$[a]	[%]	daf[d]	0.00	31.19	47.49	0.00	26.65	46.87
C	[%]	daf	48.86	56.50	62.28	49.30	59.16	66,72
H	[%]	daf	5.64	5.13	4.81	5.66	5.44	5.10
N	[%]	daf	0.23	0.32	0.35	0.38	0.46	0.53
S	[%]	daf	0.02	0.00	0.01	0.00	0.04	0.06
O[b]	[%]	daf	45.25	38.05	32.55	44.66	34.90	27.59
Ash	[%]	dry	0.36	0.66	0.96	1.30	2.06	2.71
Water	[%]	ar[e]	7.28	2.00	1.64	7.30	3.94	3.78
Volatiles	[%]	daf	85.34	71.25	58.58	83.36	67.84	54.44
Fixed carbon[b]	[%]	daf	14.66	28.75	41.42	16.64	32.16	45.56
d_{10}	[µm]		76.2	86.1	83.5	60.0	73.0	63.8
d_{50}	[µm]		103.8	105.3	105.2	90.7	90.0	84.6
d_{90}	[µm]		150.9	137.6	133.3	118.8	117.0	106.1
Mean sphericity Ψ[c]	[−]		0.52	0.63	0.63	0.45	0.60	0.62

[a] See equation (3).
[b] From difference.
[c] See equation (4).
[d] Reference state: dry, ash-free.
[e] Reference state: as received.
[f] Before drying.

of volatiles combined with a decrease of oxygen and hydrogen. This is caused by decomposition of the three major components – hemicellulose, cellulose and lignin [27].

The changes in carbon, hydrogen, and oxygen fractions are shown in a Van Krevelen diagram, plotting atomic ratios of H/C over O/C [39], depicted in Fig. 6.

The diagram reveals a decrease of O/C and H/C ratios for torrefied biomass compared to raw biomass, which is mainly driven by the reduction of hydroxyl (−OH) groups [40]. A higher torrefaction temperature reinforces the effect, which was also reported by Gucho et al. [41], Park et al. [42], Phanphanich and Mani [40] and Xue et al. [43]. For high torrefaction temperatures, the residual material comes close to the elemental composition of coal, especially lignite [42,44–47]. As

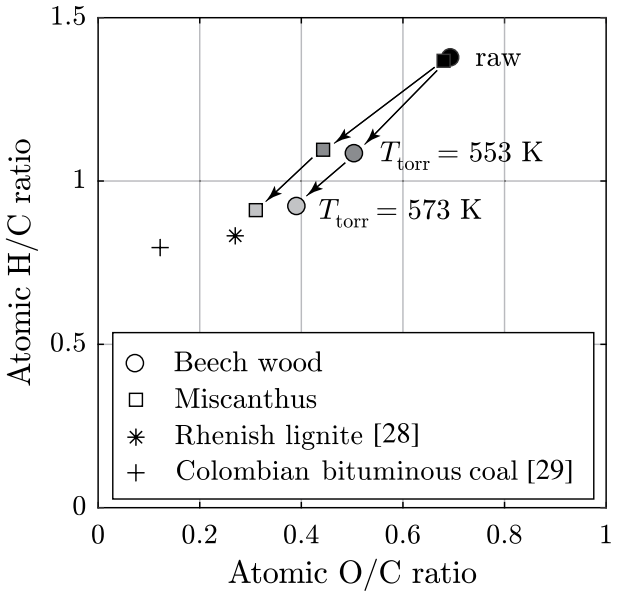


Fig. 6. Van Krevelen diagram of investigated fuels and reference fossil fuels.

remarked by Gucho et al. [41], the torrefied biomass shows differences in mass loss and energy density to lignite, although the chemical composition is quite similar. Additionally, differences in the composition of released fast pyrolysis products from torrefied biomass and lignite have been observed. A detailed investigation of fast pyrolysis products from torrefied biomass compared to those from a Rhenish lignite and a Colombian bituminous coal has been undertaken with the same reactor concept [28]. These two fossil fuels are additionally depicted for reference in the Van Krevelen diagram in Fig. 6.

Regarding particle size and shape, the torrefaction process generally leads to a shift from longer, cylindrical particles to smaller more spherical particles. This effect can be seen in the logarithmic particle size density distribution given in Fig. 7 for beech wood. As a cylindrical particle model is used, distributions can be calculated for the particle diameter and the particle length. The diameter distribution is almost identical for raw and pretreated fuel resulting from the same used mesh size in the sieving procedure. In contrast, the length distribution shifts from longer particles to shorter ones with increasing degree of torrefaction. Similar trends can also be observed for miscanthus in Fig. A.15 in the appendix.

A better indication for particle shape change is given by the mean particle sphericity Ψ proposed by Phanphanich and Mani [40].

$$\Psi = \frac{\sqrt{\frac{4 \cdot A_p}{\pi}}}{\frac{C_p}{\pi}}. \tag{4}$$

Ψ represents the diameter ratio of a spherical particle with equivalent projection area A_p and a spherical particle with equivalent circumference C_p. The torrefaction process leads to an increase of sphericities from Ψ= 0.52 to Ψ= 0.63 for beech wood and from Ψ= 0.45 to Ψ= 0.62 for miscanthus (see Table 2). The trends observed are comparable to the results obtained by Phanphanich and Mani [40], where the sphericity increased from Ψ= 0.48 to Ψ= 0.62 for pine chips. A reason for this is the improved grindability of torrefied fuels, mainly due to a breakdown of fibrous compounds as stated by several authors [13,31,40,48].

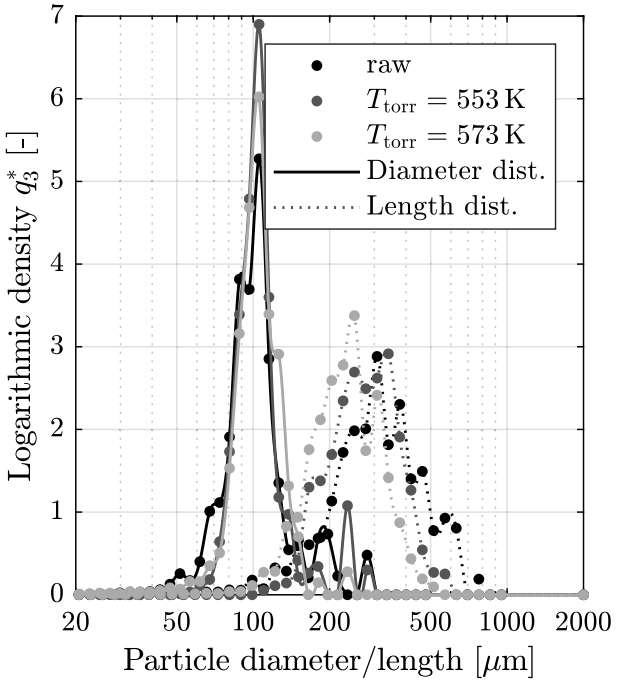


Fig. 7. Logarithmic particle size density distribution q_3^* for raw and torrefied beech wood after grinding and sieving (mesh size fraction 90–125 µm).

3.2. Residual char yield

After looking at the changes in basic fuel properties, all following sections deal with the results of the pyrolysis experiments undertaken in the fluidized bed reactor. Fig. 8 shows the yield of solid char residue calculated from the burnout phase (see Fig. 4) as a function of FBR temperature. The grayscale values of the markers indicate the degree of torrefaction as defined in equation (3). Results from this experimental study are marked with larger circles, while selected literature studies

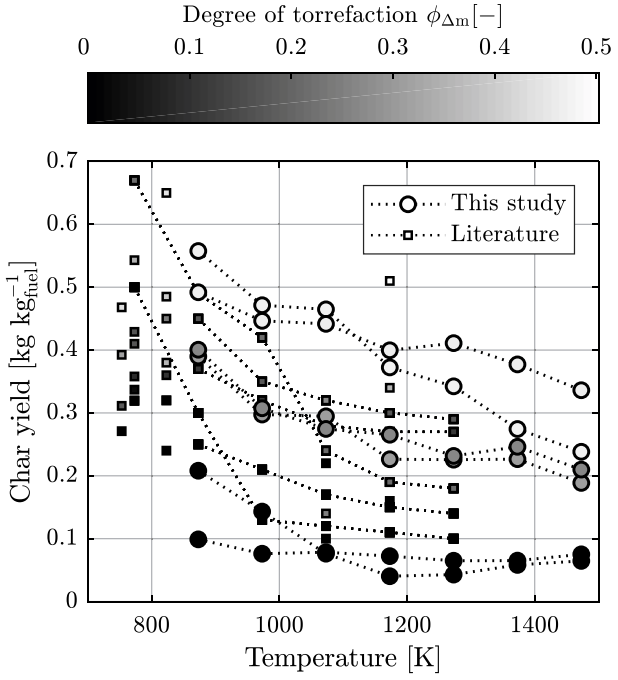


Fig. 8. Dependency of char yield from pyrolysis temperature and degree of torrefaction for selected literature data ([7,8,10,11,13–18,23]) from Table 1 and own experimental investigations.

from Table 1 are depicted as smaller squares. Both, literature data and experimental results reveal the same trends concerning the influence of torrefaction and pyrolysis temperature.

3.2.1. Influence of the degree of torrefaction

At all pyrolysis temperatures, the char yield increases with increasing degree of torrefaction (lighter colored markers). To explain this, the impact of torrefaction on the lignocellulosic components as well as their contribution to the char yield have to be considered. As shown by Ru et al. [15] and Zheng et al. [24], torrefaction leads to an increase of the lignin fraction, a strong decrease of the hemicellulose and a slight decrease of the cellulose fraction in the fuel. Zheng et al. [27] investigated, how the three components contribute to the pyrolysis yields. As lignin is the major contributor in the pyrolysis char yield, this yield increases accordingly with the degree of torrefaction [7,14,22,25]. Furthermore, increased char yields can also be attributed to cross-linking reactions between polymers of cellulose during torrefaction resulting in a more stable carbon matrix [19,21,24,25].

3.2.2. Influence of pyrolysis temperature

The variation of pyrolysis temperature reveals a decreasing char yield with increasing temperature. Overall, a stronger dependency can be observed for temperatures below 1173 K. For higher temperatures, char yields stay almost constant for raw biomass and decrease only slightly for the torrefied samples. A possible reason for this might be the decomposition temperature range of lignin. As stated by Chen et al. [10], lignin decomposition is present up to 1173 K, which will result in constant char yields at higher temperatures. This finding is supported by the elemental balance during char combustion, where small amounts of hydrogen are found up to 1173 K, but only carbon is detected above this temperature.

A similar behavior was obtained by Tsalidis et al. [16] who reported that raw biomass reaches a stagnation of the char yield – described as the end of devolatilization in their study – at lower temperatures than the pretreated fuel. The authors explained this behavior with different reactivities of the components at different temperatures. The same temperature behavior and almost identical char yields have also been obtained in studies, where only raw beech wood is investigated [49–51].

3.3. Volatile yield

Released volatiles form the counterpart to the residual char yield: Due to the normalization, the sum of char and volatile yields is one for all experiments. The volatiles are further categorized into light gases and tar. Light gas is the sum of all detected gas species with an evaporation temperature above 293 K at atmospheric pressure, plus water vapor. The latter represents an exception as the evaporation temperature of water is 373 K but it is often treated as a light gas species in the literature. The remaining detected gas species are summed up as tar. The exact assignment of each single gas species to the previously described categories can be seen in Table 3.

Fig. 9 shows the dependency of gas and tar yields from the pyrolysis temperature for raw and torrefied beech wood and miscanthus. In contrast to the char yield, only literature data of the raw fuel is plotted to compare the temperature trends and effects of gas residence time.

Table 3
Overview of gas species summed up in the cumulative gas and tar yields.

Category	Included species
Gas	CO, CO_2, NO_2, SO_2, CH_4, C_2H_6, C_2H_4, C_2H_2, C_3H_6, C_3H_8, CH_2O, H_2O
Tar	CH_4O, C_2H_4O, $C_2H_4O_2$, C_2H_6O, C_3H_6O, C_3H_4O, C_6H_6, C_7H_8, C_8H_8, $C_{10}H_8$

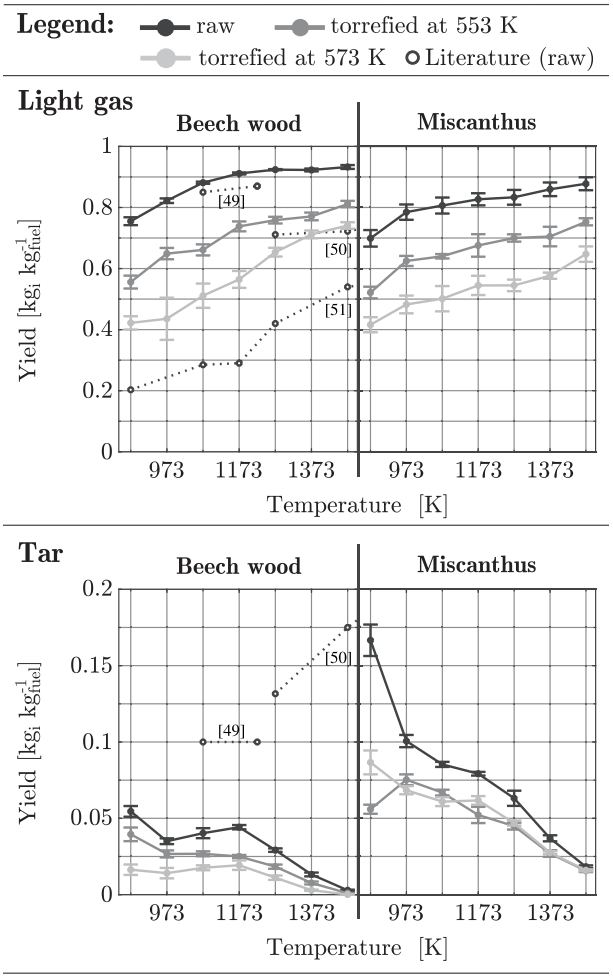


Fig. 9. Volatile pyrolysis products divided into the light gas and tar fraction, obtained from raw and torrefied (at 553 and 573 K) beech wood and miscanthus samples pyrolyzed in the temperature range of 873–1473 K.

3.3.1. Influence of gas residence time

Before analyzing the effects of torrefaction in more detail, the impact of gas residence time on gas/tar distribution is highlighted. A comparison of the yields from raw biomass with available literature data reveals partially large deviations. E.g. at 1073 K a gas yield of 0.88 kg_{Gas} kg_{fuel}^{-1} for raw biomass was obtained in this study, while literature values range from 0.86 kg_{Gas} kg_{fuel}^{-1} reported by Chen et al. [49] down to 0.29 kg_{Gas} kg_{fuel}^{-1} obtained in the study of Zeng et al. [51]. Corresponding tar yields for both studies are 0.1 kg_{Tar} kg_{fuel}^{-1} [49] and 0.63 kg_{Tar} kg_{fuel}^{-1} (out of range in Fig. 9) [51].

The main factor influencing the light gas to tar ratio is the residence time of volatile components under hot conditions. A large residence time forces secondary pyrolysis reactions including decomposition of tars towards lighter gas species. Lower gas yields from Zeng et al. [51] might be explained by the immediate cooldown of the gaseous products in the used solar furnace and the consequently shorter gas residence time at high temperature compared to those in the drop tube reactors used by Chen et al. [49] and Septien et al. [50]. A review of the residence time distribution (see Fig. 5) shows that realized gas residence times for the FBR setup are significantly larger than those in the DTR and the solar reactor. Thus the effect of secondary pyrolysis reactions is more pronounced in the FBR.

A comparison of the results for beech wood, which were obtained without the ceramic blocking in the reactor, and those for miscanthus, where the blocking was in place, reveals larger tar yields and lower gas yields for the experiments undertaken with the shorter gas residence time (→ miscanthus, cf. Figs. 5 and 9). Most likely the ceramic blocking reduces the occurrence of secondary pyrolysis reactions in the FBR. Furthermore, the different methods used for determining the tar yield have to be considered: While the yield is obtained via condensation and weight measurement in the mentioned literature sources, this study relies solely on gas analysis with an FTIR spectrometer. The method used in this study has the restriction that complex aromatic compounds with more than two carbon rings are not analyzed, resulting in a deviation of the measured yields.

Both influence factors on the tar yield – residence time and non-detection in the gas analysis – have to be considered when utilizing this data set for the development of pyrolysis models, as suggested in the introduction. However, using the residence time distribution shown in Fig. 5 can potentially be used to calculate the influence of secondary pyrolysis reactions on the effectively measured gas composition.

3.3.2. Influence of the degree of torrefaction

The influence of torrefaction on the biomass gas and tar yield is the same for all pyrolysis temperatures: Both yields decrease with increasing degree of torrefaction. For tar, this trend is verified by almost all literature studies (see. Table 1), while for gas, this trend is not observed by all investigators [10,13,17–19,26]. All these studies have pyrolysis temperatures of more than 873 K in common. In contrast, all remaining studies from Table 1 are undertaken at lower pyrolysis temperatures and report a constant or increasing gas yield with increasing degree of torrefaction. A direct confirmation of this behavior is not possible with the present data as the minimum investigated temperature is 873 K.

The temperature dependent gas release behavior might be explained with overlapping decomposition processes of lignin and cellulose. As stated by Chen et al. [10], lignin pyrolysis takes place in the temperature range from 433 to 1173 K, while cellulose pyrolysis is happening in the temperature range from 588 to 673 K. In contrast, hemicellulose is already fully decomposed at temperatures around 588 K [10]. This would also explain why trends of tar yield are not that temperature dependent as the tar formation mainly depends on hemicellulose decomposition. This comparably low-temperature decomposition process during pyrolysis is also the main reason for the drastic decrease of the tar yield with increasing degree of torrefaction [27].

3.4. Tar composition

Apart from the absolute tar yield, the relative tar composition is of great interest especially for estimating its effect on pollutant formation and the volatile heating value. The latter will be discussed in section 3.7. Fig. 10 depicts the mass fractions of condensable products (except H_2O) grouped by functional groups in the molecule. The first 3 bars represent results from miscanthus at 873 K followed by results from beech wood experiments for different pyrolysis temperatures. The data is sorted by pyrolysis temperature (see top abscissa). For each temperature, data for the raw fuel ("raw") as well as for the pretreated fuels (numbers correspond to torrefaction temperature in K) are grouped. As only results with a constant torrefaction hold time are used at each pyrolysis temperature, an increase in the torrefaction temperature (bottom abscissa) corresponds to an increase in the degree of torrefaction.

First of all, no relevant effect of torrefaction on tar composition can be identified, neither in the beech wood experiments nor in those with miscanthus. This observation is quite uncommon as several authors have reported an impact of torrefaction on the composition of condensable species – either called tar or (bio)oil in those publications. Typically, the decomposition of hemicellulose during torrefaction lowers the fraction of acids [7,9,10,25], while the increased lignin fraction after torrefaction causes a elevated release of aromatic compounds during pyrolysis [7,9,10,14,25].

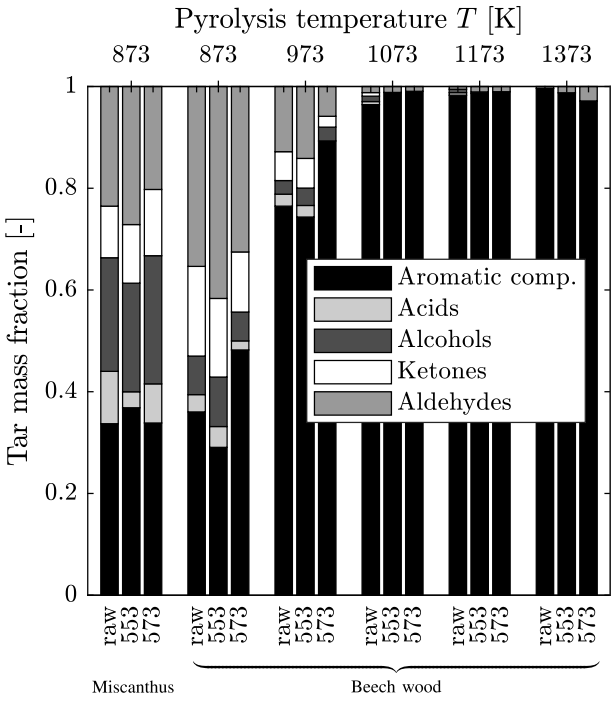


Fig. 10. Tar composition for raw and differently torrefied (label numbers indicate torrefaction temperature in K) biomass samples at different pyrolysis temperatures.

Differences between literature results and the FBR experiments may occur due to the different analysis methods: While most studies use a combination of gas chromatography and mass spectrometry (GC-MS) in which liquid oil components are analyzed after condensation [7,9,10,14,25], this study analyses the tar components in the gas phase using an FTIR without previous condensation. Thus potential reactions between different tar components are evolving differently. Furthermore, the FTIR gas analysis is limited to a lower number of species compared to a GC-MS setup to guarantee a stable evaluation procedure.

In contrast to the inconclusive correlation with the degree of torrefaction, tar composition strongly depends on pyrolysis temperature and gas residence time in the hot zone of the reactor. For temperatures below 1073 K, the composition is dominated by oxygen-containing functional group molecules (aldehydes, ketones, alcohols, acids) mainly originating from hemicellulose and cellulose decomposition [52]. With increasing temperature, the fraction of aromatic compounds increases strongly, which can be attributed to the decomposition of lignin molecules up to 1173 K. The change in residence time – represented by miscanthus (shorter residence time) and beech wood (longer residence time) – seems to affect mostly the alcohols which will decompose into H_2 and the more stable aldehydes.

Furthermore, tar components allow conclusions on potential particle emissions from combustion processes. Typically, polycyclic aromatic hydrocarbons (PAHs) serve as precursors for soot formation. As shown in Fig. B.19, the absolute amount of naphthalene (the only PAH component in this study) is significantly lower for the torrefied samples compared to the raw biomass. Impact of torrefaction on gaseous pollutant emissions such as SO_2 or NO_x is hard to evaluate as fractions of fuel S and N are quite in low in the investigated biomass (cf. Table 2) and thus concentration peaks cannot be differentiated from noise.

The clear temperature trend shows that the gas analysis itself is capable of delivering reliable results for tar composition with the known restriction that certain longer-chained hydrocarbons are currently not being analyzed. This supports the finding that no correlation between the degree of torrefaction and tar composition is observable in the results of this study.

3.5. Gas composition

Following the discussion of the overall gas yields in section 3.3, the composition of the released gases is of interest, too. Similar to the tar composition, the composition of light gases is equally important to determine the overall volatile heating value discussed in section 3.7. The light gas composition is also the most important measurement for the development of pyrolysis models, which is one of the possible applications for the data presented in this study.

For the following discussion of the influence of pyrolysis temperature and the degree of torrefaction on light gas composition, those yields combined with results from other authors have been aggregated into an easy to grasp diagram shown in Fig. 11. The labeling structure of the abscissa is identical to that used in Fig. 10 (pyrolysis temperature at the top, torrefaction temperature at the bottom).

3.5.1. Influence of the degree of torrefaction

Looking at the trends for different gas species in Fig. 11, the CO_2 fraction is increasing with the degree of torrefaction, whereas the CO fraction shows a corresponding decrease. Both trends are more pronounced at temperatures below 1173 K and are also supported by results from Chen et al. [10] and Barontini et al. [5]. The pyrolysis results of Cen et al. [7] at 773 K show an opposing trend, but there are only two

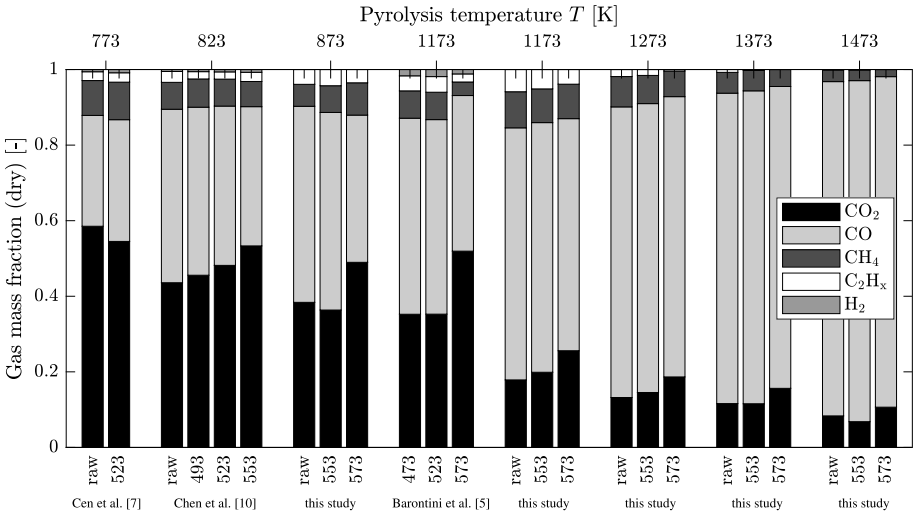


Fig. 11. Dry gas composition for raw and torrefied beech wood samples at different pyrolysis temperatures compared to literature data.

data points available from this source. Results indicate that the increase in the CO_2 fraction is most significant when the torrefaction temperature is increased from 553 to 573 K, which happens to be close to the pyrolysis temperature range of cellulose (588–673 K, cf. section 3.3). A connection of the increased CO_2 release to this process is likely.

Based on current results, the CH_4 fraction in the dry gas is not clearly linked to the degree of torrefaction. At certain pyrolysis temperatures, a weak dependency is visible in the data, but deviations are within the measurement precision. The same is true for H_2, where Cen et al. [7] and Chen et al. [10] report a slight increase of hydrogen release with the degree of torrefaction, whereas the results of Barontini et al. [5] are inconclusive. In this study, hydrogen is not measured directly. Hence, the hydrogen yield and mass fraction can only be estimated via the difference between the fuels' elemental hydrogen content (from ultimate analysis) and the hydrogen mass in all detected gas species. These estimates (not shown in Fig. 11) indicate a slightly increasing trend of the hydrogen fraction with the degree of torrefaction. However, the hydrogen-by-difference estimates possess a high degree of uncertainty.

For the last light gas species listed in Fig. 11, the sum of short-chained hydrocarbon species C_2H_x, a slight decrease of the gas fraction with the degree of torrefaction is found in this study. This result is further supported by most of the listed data points from the literature [5,11] (see Table 1).

3.5.2. Influence of the pyrolysis temperature

The influence of pyrolysis temperature on individual light gas fractions overall is more pronounced than the influence of the degree of torrefaction. For all experiments in this work, as well as all sources listed in Fig. 11 ([5,7,10]), the temperature trends are clear: The CO_2 and CH_4 fractions decrease with increasing pyrolysis temperature, while the CO fraction increases markedly. The hydrocarbon (C_2H_x) mass fraction of the light gas is also decreasing. Based on data from the literature and the hydrogen-by-difference estimates in this work, the H_2 fraction of the dry gas monotonically increases with the pyrolysis temperature. For the experiments in this work, the trend of an increasing hydrogen mass fraction is more pronounced above 1073 K than below this temperature.

3.6. Chemical equilibrium analysis of gas phase components

In the previous sections the impact of torrefaction and pyrolysis temperature on gas and tar composition is discussed. This section presents two different approaches to correlate the measured yield behavior of single gas species with molecule specific properties.

The temperature-dependent yield curves of most hydrocarbon gas species (see Figs. B.17–B.19) show a qualitatively similar behavior: A parabolic trend with a maximum located at a certain temperature T_{peak} and an amplitude scaling with the degree of torrefaction. T_{peak} seems to be independent of the fuel, as raw miscanthus and beech wood as well as the torrefied samples and also fossil fuels (see Pielsticker et al. [28]) all show the same parabolic relationship between yield and temperature. This indicates that the yield maxima are not primarily controlled by the kinetics of the decomposition reactions but might instead be dominated by the thermodynamic equilibria of secondary gas phase reactions.

To investigate whether the gas composition detected in the FTIR is dominated by primary pyrolysis or by secondary gas phase reactions, two alternative approaches are used: A chemical equilibrium analysis for a sub-set of gas phase components is undertaken to estimate T_{peak}. As an alternative to the equilibrium method, the bond dissociation energy of the weakest bond in each species is calculated and compared with the species' T_{peak} from the experimental data.

As a detailed study taking all possible gas phase reactions into account would go beyond the scope of this work, a selection of the C_2H_x species ethane, ethylene, acetylene is used for a proof of concept. To quantify on which side of the reaction the equilibrium is established, the Gibbs free reaction energy ΔG_{reac} is used.

$$\Delta G_{reac} = \sum \Delta G_{prod} - \sum \Delta G_{ed} \tag{5}$$

If the Gibbs free reaction energy equals zero, educts and products are in equilibrium, whereas a positive Gibbs free reaction energy represents a shift in favor of the educts and vice versa. The Gibbs free reaction energies for each reaction ΔG_i are calculated at temperature T via the simplified equation (6), where enthalpy ΔH_i and entropy ΔS_i at standard conditions are taken from literature [53] and are assumed to be temperature independent.

$$\Delta G_i = \Delta H_i - T \cdot \Delta S_i \tag{6}$$

The equilibrium of a reaction is not only influenced by the Gibbs free reaction energy, but also by the individual concentrations c_i of all species involved in the reaction. This phenomenon can be described with the equilibrium constant K defined by equation (7).

$$K = \exp\left(\frac{-\Delta G_{reac}}{R \cdot T}\right) = \frac{\prod_{prod} c_i^{\nu_i}}{\prod_{ed} c_i^{\nu_i}} \tag{7}$$

In here, R is the universal gas constant and ν_i is the stoichiometric coefficient of species i. The chemical equilibrium itself has not been computed, because the a-priori concentrations of the educts in the gas phase are unknown.

Instead, calculated Gibbs free reaction energies of the three potential reactions (Equations (8)–(10)) are compared to the measured yields in Fig. 12. To avoid cluttering the plot with too many results, only normalized yields (max. yield per species = 1) for raw miscanthus are shown.

$$C_2H_6 \rightleftharpoons C_2H_4 + H_2 \tag{8}$$

$$C_2H_6 \rightleftharpoons C_2H_2 + 2H_2 \tag{9}$$

$$C_2H_4 \rightleftharpoons C_2H_2 + H_2 \tag{10}$$

For ethane, the maximum yield is detected at 973 K or lower where the Gibbs free energies of all reactions are positive. With rising

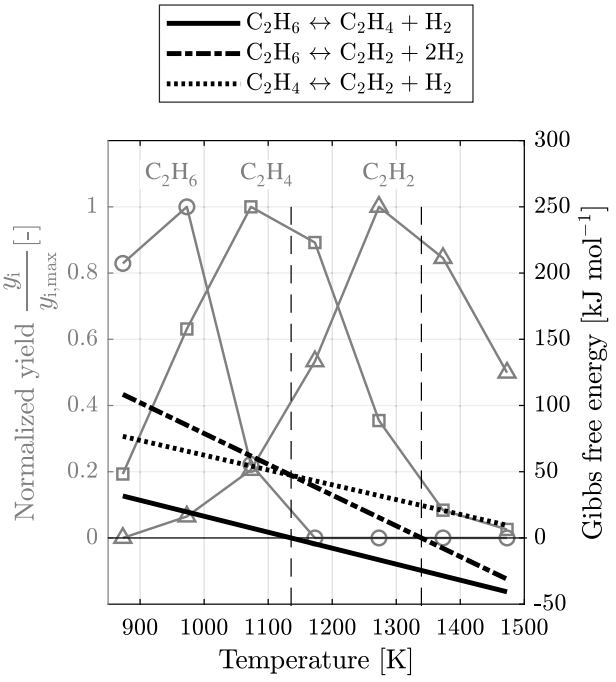


Fig. 12. Normalized yields of C_2H_x species of raw miscanthus (gray curves, left axis) in correlation with Gibbs free energy of potentially involved reactions (black curves, right axis).

temperature, the Gibbs energies reduce and the reaction equilibria shift towards the products. The yield maxima of ethylene and acetylene are detected at 1073 K and 1173–1273 K respectively. The Gibbs free energy for the reaction ethane-ethylene (Eq. (8)) equals zero at 1136 K, that of the reaction ethane-acetylene (Eq. (9)) switches sign at 1339 K. The equilibrium for the reaction ethylene-acetylene (Eq. (10)) is at 1558 K. In consequence, the latter reaction does not strongly influence the gas composition in the investigated temperature range.

Based on the laws of chemistry, yield maxima of reaction products are expected at temperatures with negative Gibbs energies. For the species C_2H_4 and C_2H_2, this is nearly the case: A slight shift of their peak towards lower temperatures is observed in Fig. 12. The impact of different gas concentrations seen in Equation (7) is ignored when only using the Gibbs free reaction energies as a basis for comparison. As products of the three investigated reaction paths (Equations (8)–(10)) are already present in the gas phase from primary pyrolysis, the equilibrium of the reaction is different from that in an ideal case where only the educts are present before the secondary pyrolysis begins. This may partly explain the observed shift of the yield maxima compared to the zero-points of the Gibbs free reaction energies. Furthermore, the investigated set of only three reactions ignores interactions with other gases like carbon monoxide, carbon dioxide or methane. Therefore, it cannot explain the reduction of the acetylene yield past 1273 K. Under these conditions, acetylene can either react with carbon dioxide to carbon monoxide and hydrogen or be consumed by a variety of reactions that eventually lead to the formation of soot and hydrogen [54]. In the presented fluidized bed experimental setup, soot cannot be detected individually and will appear to be part of the char. The amount of soot formed during pyrolysis is therefore unknown and cannot be used to investigate these reaction pathways.

As an alternative route to explain the observed peak temperature T_{peak} for each species, an approach considering the energy in the weakest bond is undertaken. Table 4 shows the dissociation energies $D_{0,298K}$ of the weakest bonds and the corresponding peak temperature T_{peak}. As it can be seen, the temperature of the maximum yield for these compounds increases with dissociation energy. The bond dissociation energies should be correlated with the activation barriers for the initial decomposition steps, which e.g. for naphthalene are followed by the formation of a variety of cracking compounds and soot [55].

Overall, the results show that gas species distribution is most likely correlated to thermodynamic gas phase equilibrium reactions and molecular stability criteria. Fuel composition seems to have less impact on relative gas species distribution but scales the yield with the amount of released volatiles.

Table 4
Bond dissociation energies of weakest R—H bond in hydrocarbon molecules in comparison with yield peak temperature measured in fluidized bed reactor.

Species	Ref.	$D_{0,298K}$ [kJ mol^{-1}]	T_{peak} [K]
Formaldehyde	[56]	369.0	<873
Propene	[57]	369.0 ± 3.0	<973
Acetaldehyde	[57]	374.0 ± 1.3	<873
Toluene	[58]	375.7 ± 2.5	<873
Ethane[a]	[56]	376.7 ± 0.2	<973
Ethanol	[59]	389.1 ± 4.2	<873
Acetic acid	[57]	398.7 ± 12.1	<873
Methane	[57]	439.3 ± 0.4	1173
Styrene[b]		440.4	973–1173
Ethylene	[56]	462.5 ± 0.3	1073
Naphthalene	[60]	468.2 ± 5.9	1173
Benzene	[61]	472.2 ± 2.2	1173
Acetylene	[56]	557.7 ± 0.1	1173–1273

[a] C-C bond is identified as weakest bond.

[b] The bond dissociation energy of the weakest bond of styrene has been calculated using CCSD(T)-F12/cc-pVTZ//B3LYP-D3/def2-TZVP using zero point energy corrections and rotational, vibrational, and translational contributions to the enthalpy at 298.15 K under rigid rotor and harmonic oscillator approximation using TURBOMOLE Quantum Chemistry package.

3.7. Heating value

Based on the yields for char (section 3.2) and volatiles (section 3.3) as well as their composition (section 3.4 and 3.5), the higher heating value (HHV) of the volatile gases and the char is computed according to equation (11). This indirect method of estimating the HHV is a novelty in biomass research and only possible thanks to the detailed gas analysis presented in section 2.5. Common methods for heating value estimation in biomass research rely either on empirical formulae using ultimate and/or proximate analysis data [62,63] or on direct measurement [7,9]. The presented HHV estimates in this study are useful for a multitude of applications – most notably for improving CFD simulations of biomass flames and boilers.

$$HHV = \sum_{i=1}^{n} y_{H_2} \cdot HHV_{H_2} + y_{pyro,i} \cdot HHV_i + y_{char,i} \cdot HHV_i \quad (11)$$

In here, HHV is the higher heating value, i is an analyzed gas species and n is the total number of species. y_{H_2}, y_{pyro} and y_{char} are the specific hydrogen, pyrolysis and char combustion gas yields per kg_{fuel}. The hydrogen yield y_{H_2} is approximated by difference based on the fuel analysis (cf. Table 2) and the total hydrogen mass detected in all pyrolysis gases and the char.

Calculated higher heating values at a pyrolysis temperature of 873 K for all fuels are presented in Fig. 13 (bars “Char”, “Vol.” and “H_2”). A temperature of 873 K has been chosen, because the formation of hydrogen gas at this temperature is still limited, which results in a more reliable estimate of the HHV. Although the amount of undetected tar, consisting mostly of long-chained hydrocarbon species, is higher at 873 K than for higher temperatures, the total undetected mass is considered minor overall. The monotonical decrease of HHV values above 1073 K (not shown) confirm this presumption as with increasing temperature tar yield decreases and yield of molecular hydrogen increases.

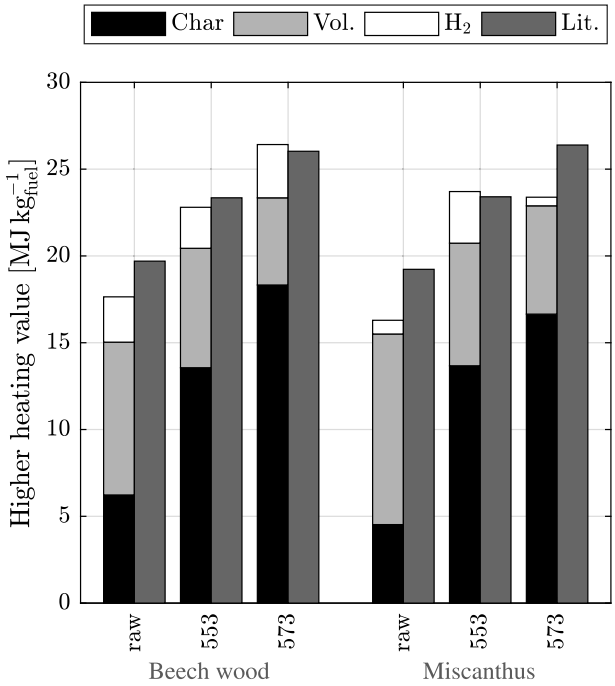


Fig. 13. Higher heating value (HHV) of hydrogen, other volatiles and char formed during pyrolysis of raw and torrefied beech wood and miscanthus at 873 K. The ’Lit.’ bar represents HHV estimations from literature sources, based on torrefaction degree for beech wood [31] and elemental composition for miscanthus [64].

Hence, the gas-analysis-based HHV estimate is most reliable at low to medium temperatures (873–1073 K).

Fig. 13 also contains an HHV estimate based on literature correlations (bar "Lit."). For beech wood, a correlation based on experimental data from Ohliger et al. [31] is used, which predicts the HHV of this fuel depending on the degree of torrefaction. For miscanthus, a generalized HHV prediction for biomass by Channiwala and Parikh [64] based on the fuels' ultimate analysis is employed. In contrast to that from Ohliger, the Channiwala correlation has not been developed for torrefied fuels, but should nonetheless give a reasonable estimate of the HHV.

Overall, calculated higher heating values fall into the range of 16.3–26.4 MJ kg_{fuel}^{-1}, which is in the same range as what other authors have found for similar raw and torrefied biofuels [7,9,14,31] (deviations are between 0 and 4 MJ kg_{fuel}^{-1}). Compared to the correlations of Ohliger et al. [31] and Channiwala and Parikh [64] (dark gray bar "Lit." in Fig. 13), the HHV estimate of this work is lower for most fuels except beech wood torrefied at 553 K and miscanthus torrefied at 573 K. The mean deviation for all six fuels is 6.1%, the maximum deviation amounts to 15.3%. Without the estimated hydrogen contribution, all calculated heating values would be lower than those predicted by literature correlations and the mean and maximum deviations would increase. Hence, the approach of calculating hydrogen by difference to the fuel analysis certainly improves the heating value prediction.

Comparing the HHV values in Fig. 13 it is evident that the total HHV (volatiles + char) increases with the torrefaction temperature and thereby with the degree of torrefaction. This effect has been widely reported in literature [7,9,14,31].

Fig. 13 also shows that the share of char in the total heating value of the fuel increases with the degree of torrefaction. The same effect has been reported by Ren et al. [14] for raw and torrefied Douglas fir. The effect is mainly caused by the loss of volatile matter during torrefaction.

As mentioned in section 3.2, torrefaction is thought to decompose a large fraction of the hemicellulose in the fuel, while cellulose only decomposes slightly and most of the lignin is preserved [15,24]. Based on a least squares fit to data from Demirbaş [62], who investigated the heating values of fourteen different raw biofuels, the higher heating values of hemicellulose, cellulose and lignin are 15.8 MJ kg^{-1}, 17.2 MJ kg^{-1} and 25.7 MJ kg^{-1} respectively.[2] This supports the hypothesis that mostly lignin is preserved after torrefaction of the fuel as the HHV estimates in Fig. 13 increase towards the value for lignin with increasing degree of torrefaction.

The specific heating value of the volatiles given in MJ kg_{volat}^{-1} (*not* MJ kg_{fuel}^{-1}) has also been calculated. This specific HHV varies between 13.3 MJ kg_{volat}^{-1} and 16.7 MJ kg_{volat}^{-1} for all volatiles including hydrogen. That of the residual char calculates to 33.2–37.1 MJ kg_{char}^{-1}. The char is mostly composed of carbon (HHV 32.9 MJ kg_{C}^{-1}) and up to 18% of ash, assuming that all fuel ash is concentrated in the char. The char hydrogen content (HHV 141.9 MJ $kg_{H_2}^{-1}$) is always below 11% and quickly approaches zero for pyrolysis temperatures above 1273 K.

As supported by Ref. [9], the specific higher heating value of the volatiles released during pyrolysis monotonically increases with the degree of torrefaction, while there is no such trend for the pyrolyzed char – values scatter around 35 MJ kg_{char}^{-1} with no apparent trend. Both results are relevant for torrefied biomass flames and boilers because the specific heating values of char and volatiles influence the local energy release from the fuel during combustion. An increased degree of torrefaction shifts the energy release from the homogeneous volatile combustion towards the heterogeneous char burnout reaction. This effect will have a significant impact on the affected timescales as oxidation of volatiles occurs with higher reaction rates than the char conversion.

4. Conclusions

In the present study, the impact of torrefaction conditions and pyrolysis temperature on fast pyrolysis products of biomass under flame-equivalent conditions is investigated. Raw beech wood and miscanthus were torrefied in a continuously working screw reactor at 553 and 573 K with a residence time of 30 min. A small-scale fluidized bed reactor working in the temperature range from 873 to 1473 K combined with an ex-situ FTIR gas analysis was used to determine mass specific pyrolysis yields of 22 gas species, which can be divided into light gas and tar components. After pyrolysis had ended, the residual char was burned and the product gas was analyzed as well. The detailed pyrolysis results are used for a deeper understanding of the present gas phase reactions. Furthermore, pyrolysis species yields in combination with char species yields are used to estimate the volatile and the char higher heating values.

First of all, most of the obtained results support known trends from the literature concerning the impact of degree of torrefaction. Based on the presented data set, observations for single pyrolysis temperatures commonly found in literature are extended to the entire investigated temperature range. The main trends are that an increasing degree of torrefaction leads to.

- increasing char yields,
- decreasing volatile yields for both, tar and gas fraction,
- increasing CO_2 and H_2 fractions at the expense of decreasing CO and C_2H_x fractions in the pyrolysis gas mixture,
- increasing total higher heating value.

All these trends are traced back to the decomposition of hemicellulose during torrefaction, resulting in a lignin and cellulose enriched fuel compared to the raw biomass.

The detailed gas analysis applied in this study extends the results concerning the impact of torrefaction to non-reported phenomena. It is found, that an increasing degree of torrefaction.

- has no significant impact on the tar composition,
- causes decreased yields of polycyclic aromatic hydrocarbons (PAHs) which are known soot precursors,
- causes changes in the higher heating values of volatiles and char, which shift the energy release from homogeneous to heterogeneous combustion.

Further on, the temperature dependent distribution of single hydrocarbon gas species results most likely from thermodynamic equilibrium reactions, while absolute yield scales with the degree of torrefaction.

The extensive, temperature dependent data set of 22 single pyrolysis gas species presented constitutes a novelty in torrefied biomass research and can be used for further development of complex pyrolysis network models as well as CFD simulations of entire boiler systems.

Acknowledgements

The authors would like to thank the German Research Foundation (DFG) for funding Stefan Pielsticker, Benjamin Gövert, Özlem Yönder and Vanessa Angenent within the SFB/Transregio 129 "Oxyflame". Furthermore, the authors would thank Mark Junker, Astrid Saβmannshausen, Sascha Scheef and Jonas Voigt for supporting the experimental investigation during their theses.

[2] All HHV values dry, ash free. Data taken from Demirbaş [62].

Appendix A. Microscopic particle size analysis

Particle size and shape distribution are analyzed based on images taken with a *Nikon D5100* digital camera and an *Olympus SZ-40* zoom stereo microscope. The microscope is equipped with a 100AL *2x* conversion lens and operated in a back-light mode, resulting in shadow images of the particles as seen in Fig. A.14.

Recorded images have resolution of 4928 px × 3264 px. The combined setup is calibrated with an etched micro meter grid, giving a resolution of 1.02 µm px^{-1} at the 2× zoom level. At this magnification, the analyzed section on the sample holder measures 5.0 mm × 3.3 mm. To obtain a reliable particle characterization, only particles of at least 5 µm diameter are considered, which corresponds to a mean diameter of 5 px in the image. To obtain statistically reliable data sets, at least 1000 particles of each sample are analyzed.

For the analysis, a small sample is uniformly spread on a Petri dish which serves as a sample holder. Images are taken randomly from different regions, avoiding image overlap and regions with strong particle agglomeration. Evaluation of the resulting images is handled in MATLAB. Images are converted into grayscale, the contrast is maximized and the image is then binarized based on a pre-set threshold. Potentially contacting particles are split using a method presented by Ref. [65]. After splitting, the MATLAB function `regionprops()` is used to identify particle properties (area, pixel list and others) in the binary image. From this information, the particle outline and other parameters are derived. Fig. A.14 shows a section of an exemplary, contrast-corrected grayscale image together with the identified particle outlines.

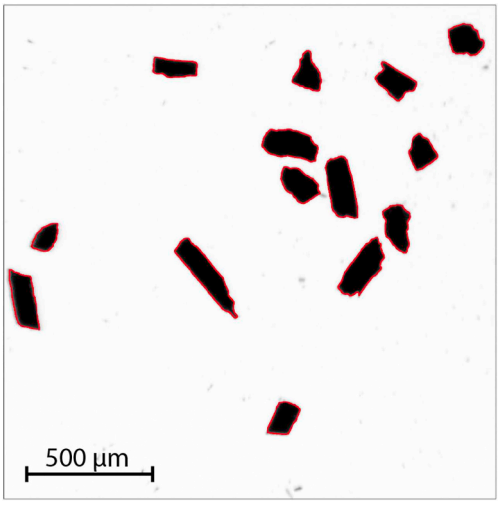


Fig. A.14. Section of shadow image and identified particle outlines (red) from the analysis of torrefied miscanthus particles (573 K, 30 min).

For the elongated biomass particles encountered in this work, the equivalent diameter is calculated using equation (A.1), postulating a cylindrical particle shape. It is further assumed that the cylinders are longer than wide and are lying flat in the image plane.

$$d_p = \sqrt{\frac{A_p}{\frac{L_{max}}{L_{min}}}} \tag{A.1}$$

In this equation, A_p is the recognized area of the particle and L_{max} and L_{min} are the lengths of the major axis and minor axis of an ellipsoid with same normalized central second moments as the particle (parameters MajorAxisLength and MinorAxisLength from `regionprops()`). The hypothetical length L_p of the cylindrical particles is calculated accordingly as

$$L_p = \frac{A_p}{d_p} \tag{A.2}$$

For generating the particle size distribution and calculating the distribution characteristics (d_{10}, d_{50}, d_{90}, mode and others), individual particle volumes are calculated using d_p and L_p. Particles are then sorted by diameter to create a logarithmic histogram with 50 bins. Fig. A.15 shows the resulting logarithmic particle size density distribution q_3^* for raw and torrefied miscanthus samples after grinding and sieving.

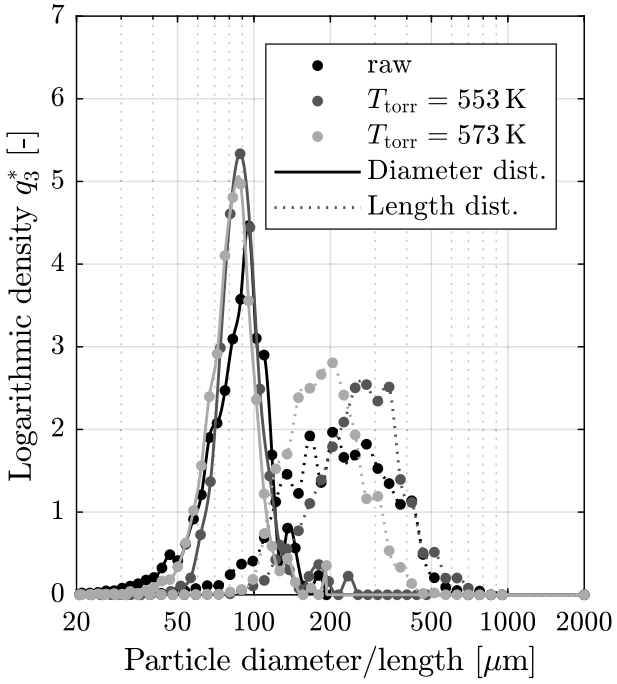


Fig. A.15. Logarithmic particle size density distribution q_3^* for raw and torrefied miscanthus after grinding and sieving (mesh size fraction 90–125 µm).

Appendix B. Single gas yields

The following graphs show the obtained species yields for both fuels with all different torrefaction degrees in dependency of pyrolysis temperature. The species have been grouped according to their molecular structure. The categories can be seen in Table B.5.

Table B.5
Overview of grouped categories for single gas species yields.

Category	Species included
Inorganic compounds	H_2O, CO_2, CO, NO_2
Light hydrocarbons	CH_4, C_2H_6, C_2H_4, C_2H_2, C_3H_8, C_3H_6
Functional group com.	CH_2O, C_2H_4O, $C_2H_4O_2$, C_2H_6O, C_3H_6O, C_3H_4O
Aromatic structures	C_6H_6, C_7H_8, C_8H_8, $C_{10}H_8$

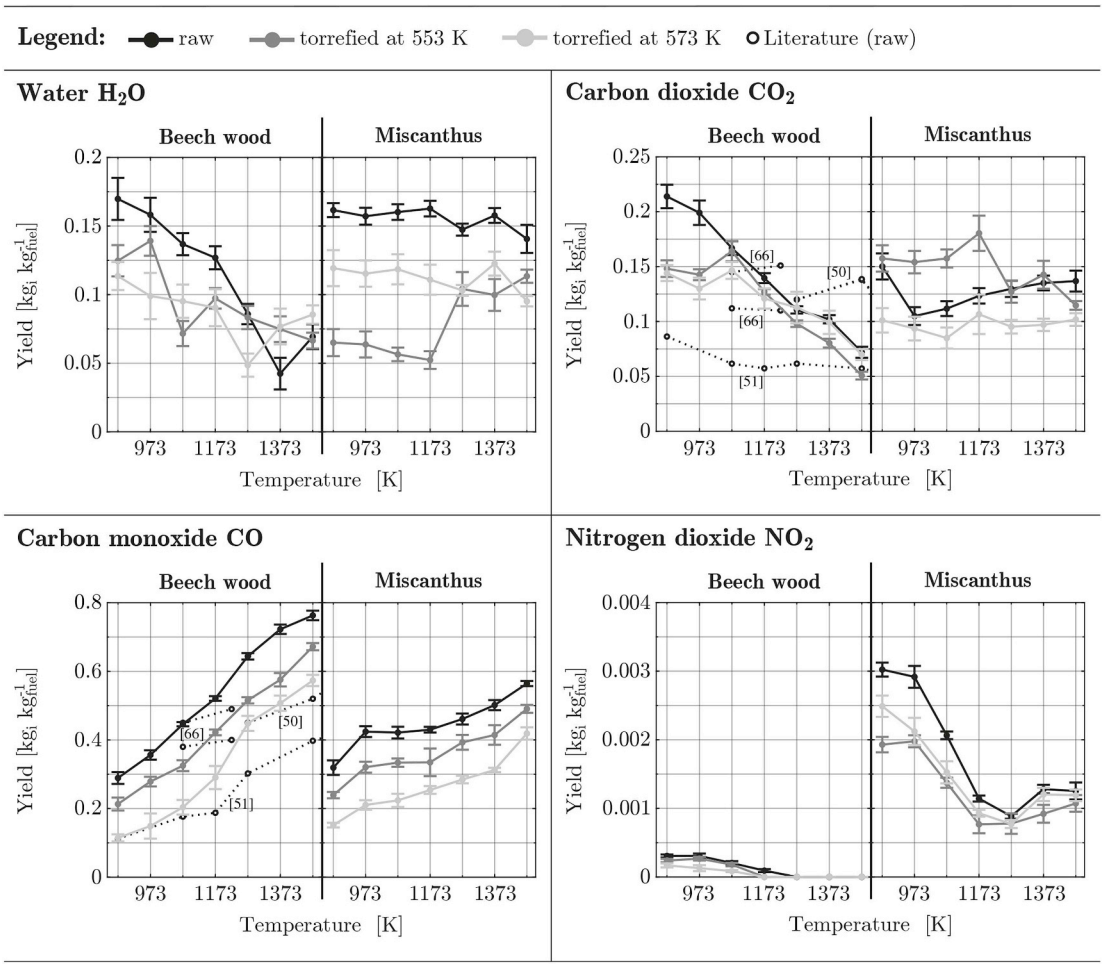


Fig. B.16. Pyrolysis yields of inorganic compounds from raw and torrefied (at 553 and 573 K) beech wood respectively miscanthus samples in the temperature range from 873 to 1473 K [Literature data: 50,51, 66].

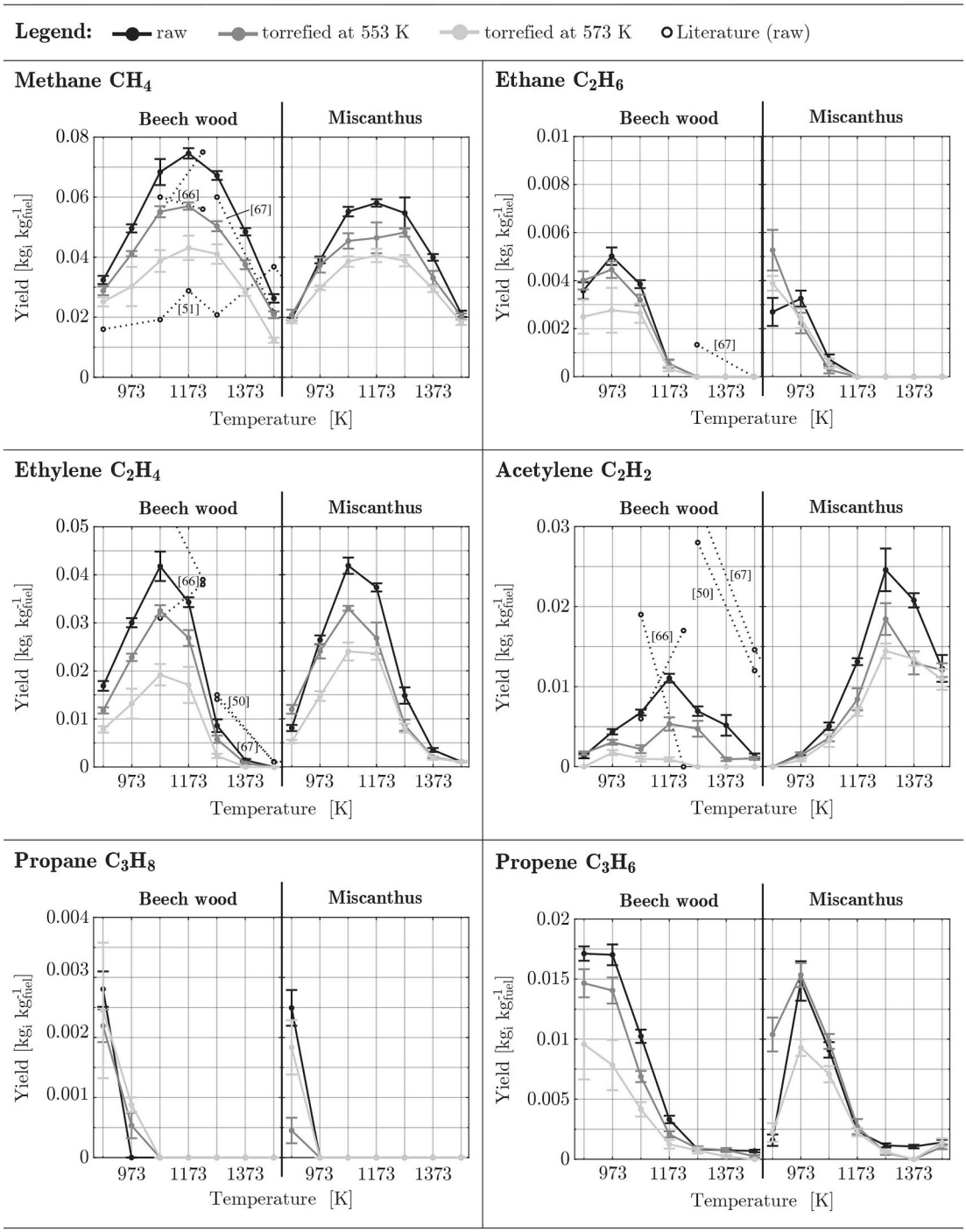


Fig. B.17. Pyrolysis yields of short-chained hydrocarbons from raw and torrefied (at 553 and 573 K) beech wood respectively miscanthus samples in the temperature range from 873 to 1473 K Literature data: [50,516667].

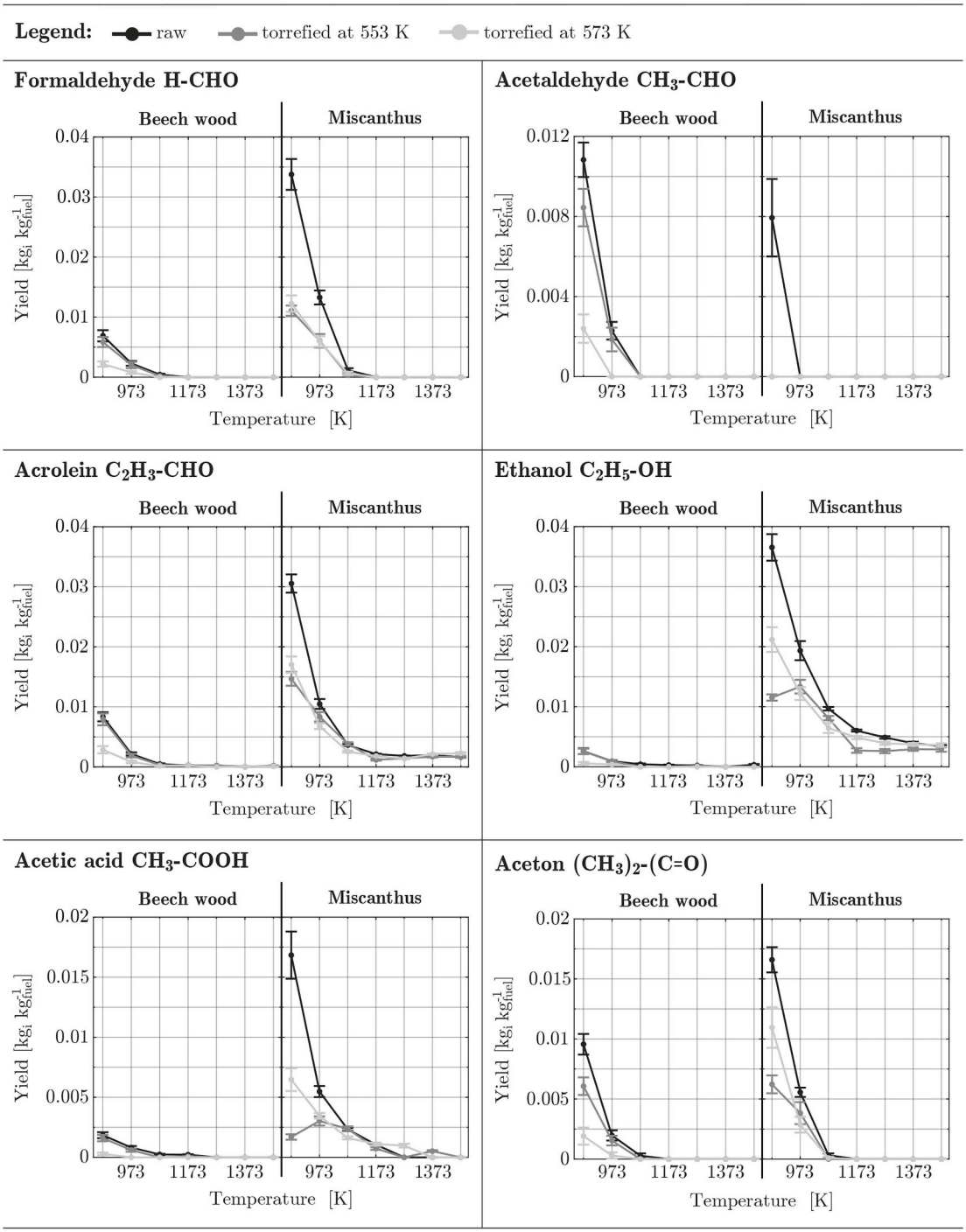


Fig. B.18. Pyrolysis yields of aldehydes, alcohols, acids and ketones from raw and torrefied (at 553 and 573 K) beech wood respectively miscanthus samples in the temperature range from 873 to 1473 K.

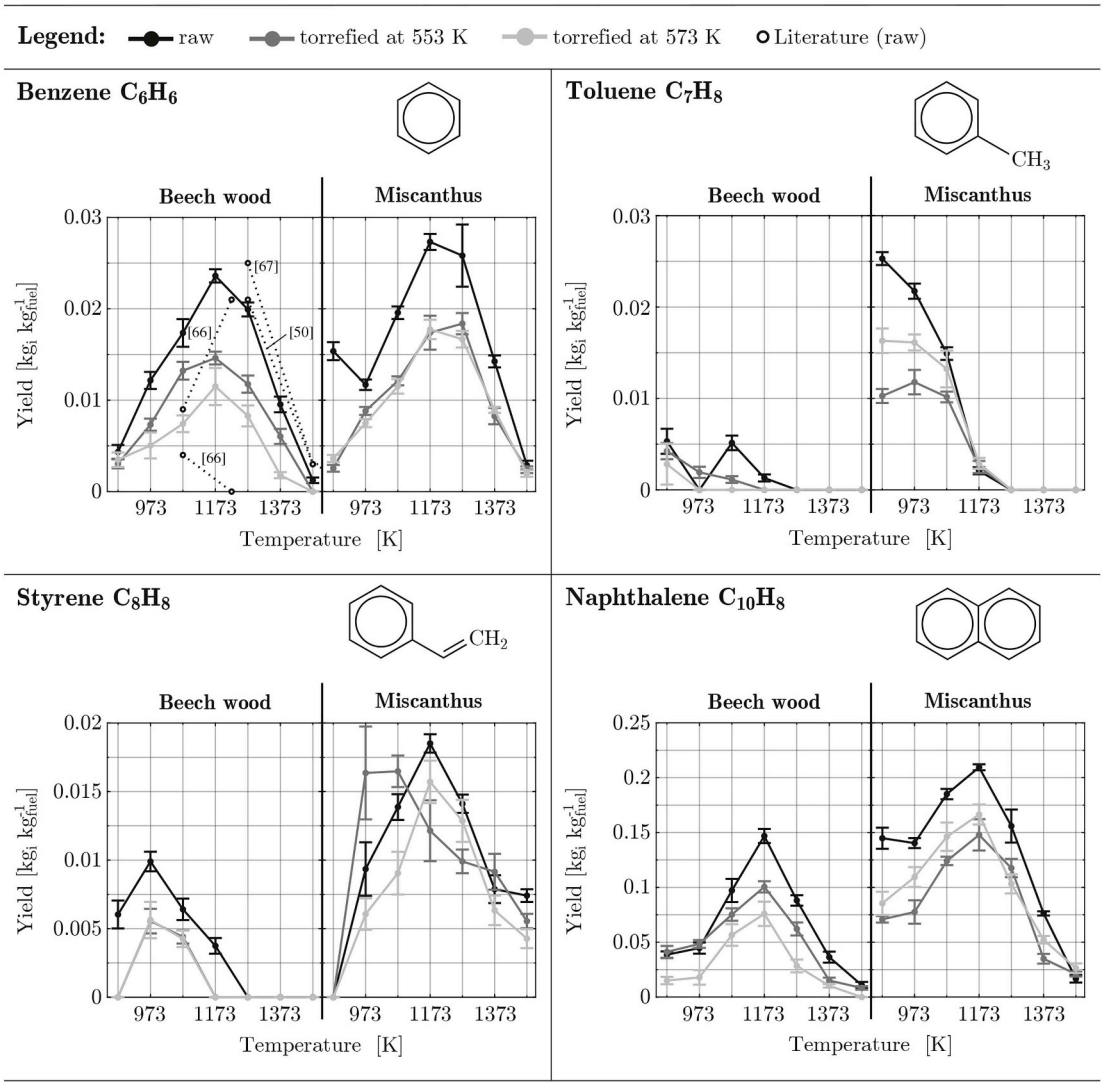


Fig. B.19. Pyrolysis yields of aromatic compounds from raw and torrefied (at 553 and 573 K) beech wood respectively miscanthus samples in the temperature range from 873 to 1473 K Literature data: [50,66, 67].

References

[1] J. S. Tumuluru, J. R. Hess, R. D. Boardman, C. T. Wright, T. L. Westover, Formulation, pretreatment, and densification options to improve biomass specifications for Co-firing high percentages with coal, Ind. Biotechnol. 8 (3), http://dx.doi.org/10.1089/ind.2012.0004.

[2] P.C.A. Bergman, A.R. Boersma, R.W.R. Zwart, J.H.A. Kiel, Torrefaction for Biomass Co-firing in Existing Coal-fired Power Stations, Energy research Centre of the Netherlands, 2005, p. 71 ECN ECNC05013 (July).

[3] J. Li, A. Brzdekiewicz, W. Yang, W. Blasiak, Co-firing based on biomass torrefaction in a pulverized coal boiler with aim of 100 % fuel switching, Appl. Energy 99 (2012) 344–354, https://doi.org/10.1016/j.apenergy.2012.05.046.

[4] F. Barontini, E. Biagini, F. Bonini, L. Tognotti, An experimental investigation on the devolatilization behaviour of raw and torrefied lignocellulosic biofuels, Chemical Eng. Trans. 43 (2015) 481–486, https://doi.org/10.3303/CET1543081.

[5] F. Barontini, E. Biagini, L. Tognotti, Characterization of the devolatilization products of selected second generation biofuels, International Flame Research Foundation, vol. 28, Freising, Germany, 2015.

[6] A. Boateng, C. Mullen, Fast pyrolysis of biomass thermally pretreated by torrefaction, J. Anal. Appl. Pyrol. 100 (2013) 95–102, https://doi.org/10.1016/j.jaap.2012.12.002.

[7] K. Cen, D. Chen, J. Wang, Y. Cai, L. Wang, Effects of water washing and torrefaction pretreatments on corn stalk pyrolysis: combined study using TG-FTIR and a fixed bed reactor, Energy Fuels 30 (12) (2016) 10627–10634, https://doi.org/10.1021/acs.energyfuels.6b02813.

[8] D. Chen, J. Zhou, Q. Zhang, Effects of torrefaction on the pyrolysis behavior and bio-oil properties of rice husk by using TG-FTIR and py-GC/MS, Energy Fuels 28 (9) (2014) 5857–5863, https://doi.org/10.1021/ef501189p.

[9] D. Chen, Z. Zheng, K. Fu, Z. Zeng, J. Wang, M. Lu, Torrefaction of biomass stalk and its effect on the yield and quality of pyrolysis products, Fuel 159 (2015) 27–32, https://doi.org/10.1016/j.fuel.2015.06.078.

[10] D. Chen, Y. Li, M. Deng, J. Wang, M. Chen, B. Yan, Q. Yuan, Effect of torrefaction pretreatment and catalytic pyrolysis on the pyrolysis poly-generation of pine wood, Bioresour. Technol. 214 (2016) 615–622, https://doi.org/10.1016/j.biortech.2016.04.058.

[11] J. Li, G. Bonvicini, L. Tognotti, W. Yang, W. Blasiak, High-temperature rapid devolatilization of biomasses with varying degrees of torrefaction, Fuel 122 (2014) 261–269, https://doi.org/10.1016/j.fuel.2014.01.012.

[12] A.C. Louwes, L. Basile, R. Yukananto, J.C. Bhagwandas, E.A. Bramer, G. Brem, Torrefied biomass as feed for fast pyrolysis: an experimental study and chain analysis, Biomass Bioenergy 105 (116–126) (2017) ISSN 0961-9534 https://doi.org/10.1016/j.biombioe.2017.06.009.

[13] M. K. Raut, P. Basu, B. Acharya, The effect of torrefaction pre-treatment on the gasification of biomass, Int. J. Renew. Energy Biofuels doi:10.5171/2016.823723.

[14] S. Ren, H. Lei, L. Wang, Q. Bu, S. Chen, J. Wu, J. Julson, R. Ruan, The effects of torrefaction on compositions of bio-oil and syngas from biomass pyrolysis by microwave heating, Bioresour. Technol. 135 (2013) 659–664, https://doi.org/10.1016/j.biortech.2012.06.091, biorefineries.

[15] B. Ru, S. Wang, G. Dai, L. Zhang, Effect of torrefaction on biomass physicochemical characteristics and the resulting pyrolysis behavior, Energy Fuels 29 (9) (2015) 5865–5874, https://doi.org/10.1021/acs.energyfuels.5b01263.

[16] G.-A. Tsalidis, K. Voulgaris, K. Anastasakis, W. De Jong, J.H.A. Kiel, Influence of torrefaction pretreatment on reactivity and permanent gas formation during devolatilization of spruce, Energy Fuels 29 (9) (2015) 5825–5834, https://doi.org/10.1021/acs.energyfuels.5b01101.

[17] G.A. Tsalidis, C. Tsekos, K. Anastasakis, W. de Jong, The impact of dry torrefaction

on the fast pyrolysis behavior of ash wood and commercial Dutch mixed wood in a pyroprobe, Fuel Process. Technol. 177 (255–265) (2018) ISSN 0378-3820 https://doi.org/10.1016/j.fuproc.2018.04.026.
[18] A. Wafiq, D. Reichel, M. Hanafy, Pressure influence on pyrolysis product properties of raw and torrefied Miscanthus: role of particle structure, Fuel 179 (2016) 156–167, https://doi.org/10.1016/j.fuel.2016.03.092.
[19] J. Wannapeera, B. Fungtammasan, N. Worasuwannarak, Effects of temperature and holding time during torrefaction on the pyrolysis behaviors of woody biomass, J. Anal. Appl. Pyrol. 92 (1) (2011) 99–105, https://doi.org/10.1016/j.jaap.2011.04.010.
[20] S. Xin, T. Mi, X. Liu, F. Huang, Effect of torrefaction on the pyrolysis characteristics of high moisture herbaceous residues, Energy 152 (2018) 586–593 ISSN 0360-5442 https://doi.org/10.1016/j.energy.2018.03.104.
[21] S. Zhang, Q. Dong, T. Chen, Y. Xiong, Combination of light bio-oil washing and torrefaction pretreatment of rice husk: its effects on physicochemical characteristics and fast pyrolysis behavior, Energy Fuels 30 (4) (2016) 3030–3037, https://doi.org/10.1021/acs.energyfuels.5b02968.
[22] S. Zhang, T. Chen, Y. Xiong, Q. Dong, Effects of wet torrefaction on the physicochemical properties and pyrolysis product properties of rice husk, Energy Convers. Manag. 141 (2017) 403–409 ISSN 0196-8904 https://doi.org/10.1016/j.enconman.2016.10.002.
[23] S. Zhang, Y. Su, D. Xu, S. Zhu, H. Zhang, X. Liu, Effects of torrefaction and organic-acid leaching pretreatment on the pyrolysis behavior of rice husk, Energy 149 (2018) 804–813 ISSN 0360-5442 https://doi.org/10.1016/j.energy.2018.02.110.
[24] A. Zheng, Z. Zhao, S. Chang, Z. Huang, F. He, H. Li, Effect of torrefaction temperature on product distribution from two-staged pyrolysis of biomass, Energy Fuels 26 (5) (2012) 2968–2974, https://doi.org/10.1021/ef201872y.
[25] A. Zheng, Z. Zhao, S. Chang, Z. Huang, X. Wang, F. He, H. Li, Effect of torrefaction on structure and fast pyrolysis behavior of corncobs, Bioresour. Technol. 128 (2013) 370–377, https://doi.org/10.1016/j.biortech.2012.10.067.
[26] A. Zheng, Z. Zhao, Z. Huang, K. Zhao, G. Wei, X. Wang, F. He, H. Li, Catalytic fast pyrolysis of biomass pretreated by torrefaction with varying severity, Energy Fuels 28 (9) (2014) 5804–5811, https://doi.org/10.1021/ef500892k.
[27] A. Zheng, L. Jiang, Z. Zhao, Z. Huang, K. Zhao, G. Wei, X. Wang, F. He, H. Li, Impact of torrefaction on the chemical structure and catalytic fast pyrolysis behavior of hemicellulose, lignin, and cellulose, Energy Fuels 29 (12) (2015) 8027–8034, https://doi.org/10.1021/acs.energyfuels.5b01765.
[28] S. Pielsticker, B. Gövert, G. Möller, O. Hatzfeld, R. Kneer, Impact of torrefaction on flash pyrolysis products of biomass and comparison to fossil fuels, 11th Asia-Pacific Conference on Combustion, Sydney, Australia, 2017.
[29] S. Pielsticker, B. Gövert, T. Kreitzberg, M. Habermehl, O. Hatzfeld, R. Kneer, Simultaneous investigation into the yields of 22 pyrolysis gases from coal and biomass in a small-scale fluidized bed reactor, Fuel 190 (2017) 420–434, https://doi.org/10.1016/j.fuel.2016.10.085.
[30] S. Pielsticker, S. Heuer, O. Senneca, F. Cerciello, P. Salatino, L. Cortese, B. Gövert, O. Hatzfeld, M. Schiemann, V. Scherer, R. Kneer, Comparison of pyrolysis test rigs for oxy-fuel conditions, Fuel Process. Technol. 156 (2017) 461–472, https://doi.org/10.1016/j.fuproc.2016.10.010.
[31] A. Ohliger, M. Förster, R. Kneer, Torrefaction of beechwood: a parametric study including heat of reaction and grindability, Fuel 104 (2013) 607–613, https://doi.org/10.1016/j.fuel.2012.06.112.
[32] Deutsches Institut für Normung e.V., DIN 51718:2002-06 Prüfung fester Brennstoffe – Bestimmung des Wassergehaltes und der Analysenfeuchtigkeit, Beuth, Berlin, 2002.
[33] Deutsches Institut für Normung e.V., DIN 51720:2001-03 Prüfung fester Brennstoffe – Bestimmung des Gehaltes an Flüchtigen Bestandteilen, Beuth, Berlin, 2001.
[34] Deutsches Institut für Normung e.V., DIN 51719:1997-07 Prüfung fester Brennstoffe – Bestimmung des Aschegehaltes, Beuth, Berlin, 1997.
[35] Deutsches Institut für Normung e.V., DIN 51732:2014-07 Prüfung fester Brennstoffe – Bestimmung des Gesamtgehaltes an Kohlenstoff, Wasserstoff und Stickstoff, Beuth, Berlin, 2014.
[36] Deutsches Institut für Normung e.V., DIN 51724:2012-07 Prüfung fester Brennstoffe – Bestimmung des Schwefelgehaltes, Beuth, Berlin, 2012.
[37] H. Haustein, T. Kreitzberg, B. Gövert, A. Massmeyer, R. Kneer, Establishment of kinetic parameters of particle reaction from a well-stirred fluidized bed reactor, Fuel 158 (2015) 263–269, https://doi.org/10.1016/j.fuel.2015.05.038.
[38] B. Gövert, S. Pielsticker, T. Kreitzberg, M. Habermehl, O. Hatzfeld, R. Kneer, Measurement of reaction rates for pulverized fuel combustion in air and oxyfuel atmosphere using a novel fluidized bed reactor setup, Fuel 201 (2017) 81–92, https://doi.org/10.1016/j.fuel.2017.03.009 .
[39] D.W. van Krevelen, Graphical-statistical method for the study of structure and reaction processes of coal, Fuel 29 (1950) 269–284.
[40] M. Phanphanich, S. Mani, Impact of torrefaction on the grindability and fuel characteristics of forest biomass, Bioresour. Technol. 102 (2) (2011) 1246–1253, https://doi.org/10.1016/j.biortech.2010.08.028.
[41] E.M. Gucho, K. Shahzad, E.A. Bramer, N.A. Akhtar, G. Brem, Experimental study on dry torrefaction of beech wood and miscanthus, Energies 8 (5) (2015) 3903–3923, https://doi.org/10.3390/en8053903.
[42] S.-W. Park, C.-H. Jang, K.-R. Baek, J.-K. Yang, Torrefaction and low-temperature carbonization of woody biomass: evaluation of fuel characteristics of the products, Energy 45 (1) (2012) 676–685, https://doi.org/10.1016/j.energy.2012.07.024.
[43] G. Xue, M. Kwapinska, W. Kwapinski, K.M. Czajka, J. Kennedy, J.J. Leahy, Impact of torrefaction on properties of Miscanthus giganteus relevant to gasification, Fuel 121 (2014) 189–197, https://doi.org/10.1016/j.fuel.2013.12.022.
[44] T.G. Bridgeman, J.M. Jones, I. Shield, P.T. Williams, Torrefaction of reed canary grass, wheat straw and willow to enhance solid fuel qualities and combustion properties, Fuel 87 (6) (2008) 844–856, https://doi.org/10.1016/j.fuel.2007.05.041.
[45] T.G. Bridgeman, J.M. Jones, A. Williams, D.J. Waldron, An investigation of the grindability of two torrefied energy crops, Fuel 89 (12) (2010) 3911–3918, https://doi.org/10.1016/j.fuel.2010.06.043.
[46] F.F. Costa, M. Costa, Particle fragmentation of raw and torrefied biomass during combustion in a drop tube furnace, Fuel 159 (2015) 530–537, https://doi.org/10.1016/j.fuel.2015.07.006.
[47] P. Rousset, C. Aguiar, N. Labbé, J.-M. Commandré, Enhancing the combustible properties of bamboo by torrefaction, Bioresour. Technol. 102 (17) (2011) 8225–8231, https://doi.org/10.1016/j.biortech.2011.05.093.
[48] B. Arias, C. Pevida, J. Fermoso, M. Plaza, F. Rubiera, J. Pis, Influence of torrefaction on the grindability and reactivity of woody biomass, Fuel Process. Technol. 89 (2) (2008) 169–175, https://doi.org/10.1016/j.fuproc.2007.09.002.
[49] L. Chen, C. Dupont, S. Salvador, M. Grateau, G. Boissonnet, D. Schweich, Experimental study on fast pyrolysis of free-falling millimetric biomass particles between 800°C and 1000°C, Fuel 106 (2013) 61–66, https://doi.org/10.1016/j.fuel.2012.11.058.
[50] S. Septien, S. Valin, M. Peyrot, B. Spindler, S. Salvador, Influence of steam on gasification of millimetric wood particles in a drop tube reactor: experiments and modelling, Fuel 103 (2013) 1080–1089, https://doi.org/10.1016/j.fuel.2012.09.011.
[51] K. Zeng, D. Gauthier, R. Li, G. Flamant, Solar pyrolysis of beech wood: effects of pyrolysis parameters on the product distribution and gas product composition, Energy 93 (2015) 1648–1657, https://doi.org/10.1016/j.energy.2015.10.008.
[52] K. Zeng, D. Gauthier, D.P. Minh, E. Weiss-Hortala, A. Nzihou, G. Flamant, Characterization of solar fuels obtained from beech wood solar pyrolysis, Fuel 188 (2017) 285–293, https://doi.org/10.1016/j.fuel.2016.10.036 ISSN 0016-2361.
[53] C.E. Mortimer, U. Müller, Chemie: Das Basiswissen der Chemie, Georg Thieme Verlag, 2007.
[54] A.A. Merkulov, A.A. Ovsyannikov, L.S. Polak, V.T. Popov, V.Y. Pustilnikov, Initial stages of soot formation in thermal pyrolysis of acetylene. I. Mechanism for homogeneous pyrolysis of acetylene, Plasma Chem. Plasma Process. 9 (1) (1989) 95–104, https://doi.org/10.1007/BF01015828 ISSN 1572-8986.
[55] A. Jess, Mechanisms and kinetics of thermal reactions of aromatic hydrocarbons from pyrolysis of solid fuels, Fuel 75 (12) (1996) 1441–1448, https://doi.org/10.1016/0016-2361(96)00136-6 ISSN 0016-2361.
[56] B. Ruscic, Active thermochemical tables: sequential bond dissociation enthalpies of methane, ethane, and methanol and the related thermochemistry, J. Phys. Chem. 119 (28) (2015) 7810–7837, https://doi.org/10.1021/acs.jpca.5b01346.
[57] Y.-R. Luo, Comprehensive Handbook of Chemical Bond Energies, CRC Press, Boca Raton (Florida), 2007.
[58] G.B. Ellison, G.E. Davico, V.M. Bierbaum, C.H. DePuy, Thermochemistry of the benzyl and allyl radicals and ions, Int. J. Mass Spectrom. Ion Process. 156 (1) (1996) 109–131, https://doi.org/10.1016/S0168-1176(96)04383-2 ISSN 0168-1176.
[59] Z.B. Alfassi, D.M. Golden, Bond dissociation energy of the carbon-hydrogen bond in ethanol. Kinetic study of the reaction iodine + ethanol, J. Phys. Chem. 76 (23) (1972) 3314–3319, https://doi.org/10.1021/j100667a003.
[60] D.R. Reed, S.R. Kass, Experimental determination of the α and β C—H bond dissociation energies in naphthalene, J. Mass Spectrom. 35 (4) (2000) 534–539, https://doi.org/10.1002/(SICI)1096-9888(200004)35:4<534::AID-JMS964>3.0.CO;2-T.
[61] K.M. Ervin, V.F. DeTuri, Anchoring the gas-phase acidity scale, J. Phys. Chem. 106 (42) (2002) 9947–9956, https://doi.org/10.1021/jp020594n.
[62] A. Demirbaş, Relationships between lignin contents and heating values of biomass, Energy Convers. Manag. 42 (2) (2001) 183–188, https://doi.org/10.1016/S0196-8904(00)00050-9 ISSN 0196-8904.
[63] R. García, C. Pizarro, A.G. Lavín, J.L. Bueno, Spanish biofuels heating value estimation. Part I: ultimate analysis data, Fuel 117 (2014) 1130–1138, https://doi.org/10.1016/j.fuel.2013.08.048 ISSN 0016-2361.
[64] S.A. Channiwala, P.P. Parikh, A unified correlation for estimating HHV of solid, liquid and gaseous fuels, Fuel 81 (8) (2002) 1051–1063, https://doi.org/10.1016/S0016-2361(01)00131-4 ISSN 0016-2361.
[65] S. Eddins, The Watershed Transform: Strategies for Image Segmentation, (2013) https://www.mathworks.com/company/newsletters/articles/the-watershed-transform-strategies-for-image-segmentation.html.
[66] L. Chen, C. Dupont, S. Salvador, G. Boissonnet, D. Schweich, Influence of particle size, reactor temperature and gas phase reactions on fast pyrolysis of beech wood, Int. J. Chem. React. Eng. 8 (1) (2010) 1–19, https://doi.org/10.2202/1542-6580.1922.
[67] S. Septien, S. Valin, C. Dupont, M. Peyrot, S. Salvador, Effect of particle size and temperature on woody biomass fast pyrolysis at high temperature (1000-1400°C), Fuel 97 (2012) 202–210, https://doi.org/10.1016/j.fuel.2012.01.049.